Fiber Optic Integration in Planar Ion Traps

by

Elizabeth Marie George

Submitted to the Department of Physics
in partial fulfillment of the requirements for the degree of

Bachelor of Science in Physics

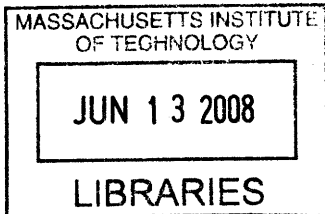at the

MASSACHUSETTS INSTITUTE OF TECHNOLOGY

June 2008

Author . . . .
Department of Physics
May 9, 2008

Certified by. . . . .
Isaac Chuang
Associate Professor, Departments of Physics and EECS
Thesis Supervisor

Accepted by . . . .
Professor David E. Prichard
Senior Thesis Coordinator, Department of Physics

Fiber Optic Integration in Planar Ion Traps

by

Elizabeth Marie George

Submitted to the Department of Physics
on May 9, 2008, in partial fulfillment of the
requirements for the degree of
Bachelor of Science in Physics

Abstract

Atomic ion traps are are excellent tools in atomic physics for studying single ions. Accurate measurement of the ion's electronic state in these ion traps is required by both atomic clocks and quantum computation. Quantum computation with trapped ions can only scale to larger numbers of qubits if the ion traps and their laser delivery and measurement infrastructure can be scaled to smaller sizes. Fiber optics are a promising method of measurement because they collect a large fraction of light scattered by the trapped ions, and many optical fibers can be placed in a small area, allowing more ions to be measured in a small region. The question I address in this thesis is, "How can optical fibers be integrated onto planar ion traps?"

This thesis presents a process I designed and implemented for integrating optical fibers onto planar ion traps as well as a system for integrating optical fibers into a cryogenic system. While the fiber integration was successful, we were unable to trap any ions in our fiber-integrated ion trap. We were able to show that the integrated fiber could collect light scattered from the surface of ion trap, and hypothesize that the large amount of dielectric present on the surface of the trap may have distorted the trapping potential and prevented us from trapping any ions. We also determined that scatter spots on the surface of the trap are a much bigger problem for fiber optic light collection systems than for traditional bulk optics systems. Finally, we propose a method of integration that could reduce the amount of exposed dielectric in the vicinity of the trap, as well as solve the problem of sensitivity to scatter spots.

Thesis Supervisor: Isaac Chuang
Title: Associate Professor, Departments of Physics and EECS

Acknowledgments

I would like to thank Yufei Ge who helped me immensely with fabrication, Shannon Wang who helped me get everything into the cryostat, attempt to trap ions, and troubleshoot, and Dave Leibrandt both for advising me and helping me troubleshoot. I also owe much graditude to Jarek Labaziewicz for being the oracle of ion trapping. I would also like to thank the entire quanta lab for providing an endless source of amusement to keep me sane.

Contents

List of Figures

List of Tables

Chapter 1

Introduction and Goals

1.1 Introduction

Atomic ion traps are are excellent tools in atomic physics for studying single particles. Among other things, they have been used for spectroscopy [IJW87], atomic clocks [RSI$^+$07, HRW07], and quantum computation [BKRB08a, WMI$^+$98, W$^+$03]. Quantum computation holds promise for large scale quantum simulations and factoring large numbers. A few groups have implemented quantum algorithms on trapped ions, such as a Molmer-Sorenson gate [BKRB08b], implemented quantum error-correction codes on trapped ions [CLS$^+$04], and realized quantum teleportation on trapped ion qubits [BCS$^+$04]. Further progress in quantum computation will require more accurate elementary operations including state measurement and scaling to more qubits.

Accurate measurement of the ion's electronic state in these ion traps is required by both atomic clocks and quantum computation. In clock experiments such as the NIST ^{27}Al$^+$ $^1S_0 \rightarrow^3 P_0$ clock transition experiment [RSI$^+$07], the state of the ^{27}Al$^+$ ion is mapped to a ^{9}Be$^+$ ion and read out via a cycling transition. However, this cycling transition is not perfectly closed, so after awhile the ^{9}Be$^+$ ion falls out of the cycling transition into another state that is not part of the measurement cycle. In order to get an accurate measurement, the measurement time needs to be much shorter than the lifetime of the cycling transition.

Quantum computation with trapped ions can only scale to larger numbers of

qubits if the ion traps and their laser delivery and measurement infrastructure can be scaled to smaller sizes. There has been great progress towards scalable ion traps in recent years with the development of microfabricated planar ion traps [S$^+$06, PLB$^+$06]. Planar ion traps are explicitly scalable to large numbers of ions in many different sites. However, the current laser delivery and measurement systems employed in experiments with planar ion traps make it impossible to address many ions at a given time.

I address both of the above technical challenges with ion traps in this thesis. The first challenge is scaling measurement systems on atomic ion traps to smaller sizes, and the second is increasing the efficiency with which measurements can be taken. Both of these challenges can be solved by integration of optical fibers onto planar ion traps. Optical fibers can be used both for laser delivery and measurement of the ion's state, and hold promise for increasing measurement efficiency of ions in planar traps.

The question I address is "How can optical fibers be integrated onto planar ion traps?" Kim and Kim [KK07] present a scalable architecture for quantum computation involving fiber optic arrays for laser delivery and ion state measurement using MEMS mirrors, lensed fibers, and micro-cavities. In 2005 Liu et al [L$^+$05] demonstrated a method for aligning fibers on a flat surface using lithography and SU-8 epoxy, with excellent results. In this thesis I attempt to use alignment structures similar to the structures Liu created to integrate fibers onto planar ion traps for ion state measurement via scattered laser light.

1.2   Overview

In this work, I first present in chapter 2 how planar ion traps work, and the ^{88}Sr$^+$ ion, which we use as our trapped ion. Section 2.2 describes the energy level structure of the ^{88}Sr$^+$ ion, cooling, and measurement of the ion.

Chapter 3 begins with the traditional approach to collection optics, then has a brief description of how fiber optics work, and ends with a description of fiber optic light collection from fluorescing ions.

With this theoretical background behind us, chapter 4 describes the microfabrication techniques we use for planar ion traps and fiber optic alignment structures, as well as integration of the fibers onto the traps.

The first half of chapter 5 describes integration of the fiber optic light collection system into the cryostat we use for experiments. The latter half explains operation of the cryostat and ion trap troubleshooting.

Chapter 6 presents our experimental results, and chapter 7 gives a conclusion to this work and an outlook for future work in the field.

1.3 Contributions to this Work

This work was done in Professor Isaac Chuang's quanta laboratory at the MIT Center for Ultracold Atoms and Research Laboratory of Electronics.

Yufei Ge assisted me with fabrication of the planar ion traps and alignment structures, Shannon Wang helped me insert my trap into the cryostat and test my ion trap and fiber optic light collection scheme, and David Leibrandt and Jaroslaw Labaziewicz helped me troubleshoot the lasers, cryostat, and ion trap when I failed to get them to work. The cryostat and laser systems were built by Jaroslaw Labaziewicz, and the planar trap was designed by Jaroslaw Labaziewicz and fabricated by Yufei Ge.

Chapter 2

Trapped $^{88}\text{Sr}^+$ Ions

Ion traps are a useful tool in various areas of atomic physics as well as other scientific disciplines. Among other things, trapped ions have been used as optical clocks [RSI$^+$07, HRW07], and several groups have used trapped ions as qubits for implementing quantum algorithms and as quantum information storage [BKRB08a, W$^+$03]. These trapped ions have future promise as a scalable platform for quantum computation. Both optical clocks and quantum computation with trapped ions require accurate ion state measurement.

This chapter discusses how a planar ion trap, first proposed by Chiaverini et al [CBB$^+$05], works in section 2.1 and also the $^{88}\text{Sr}^+$ ion in section 2.2. The chapter goes over level structure and the lasers we use to address transitions between these levels, various cooling methods we use when trapping ions, and measurement of the ion's state.

2.1   How a Planar Ion Trap Works

The planar ion traps we use [PLB$^+$06] are Paul traps, which use an electric field oscillating at radio frequencies to create a trapping potential [POF58]. There are many geometries of Paul traps, including linear-quadrupole (4-rod) traps and Paul's original design, which was a ring with two endcaps. The trap geometry which is most analogous to a planar trap is a 4-rod geometry. The equations to describe the trapping

potential are the same in both a 4-rod trap and a planar trap. Planar traps have trapping potentials which are shallower than 4-rod traps for similar values of voltages used. This makes trapping ions more difficult, and contributes to shorter ion lifetimes in the traps. However, the planar geometry is excellent for optical integration and scaling. For clarity, this section will first describe a 4-rod trap, and then will show how a 4-rod geometry extends to a planar geometry.

2.1.1 The 4-rod trap

4-rod traps have 2 rods which are driven are RF, and 2 which are grounded. The oscillating RF field creates a potential which confines the ions to the central axis of the trap. The ends of the rods have sections which can be kept at a static positive DC voltage to provide an axial confinement potential as well. These end segments of the rods can also be replaced by endcaps kept at a positive DC voltage which serve the same purpose. Figure 2-1 shows a cross section of a 4-rod trap and a side view of a 4-rod trap with endcaps.
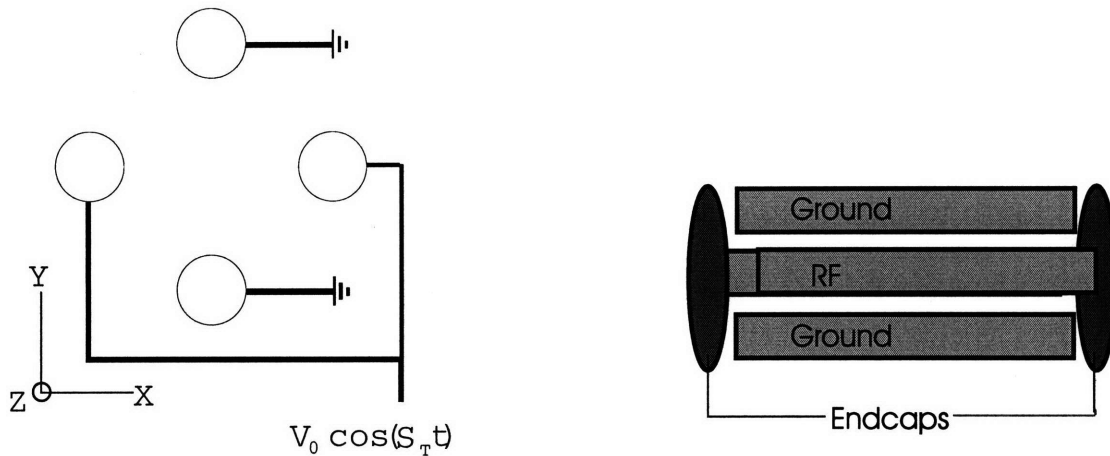

Figure 2-1: Left: Cross section of a 4-rod trap. $(S_T = \Omega_T)$ Right: Side view of a 4-rod trap with end-caps. Drawings are not to scale.

The end caps at a positive DC voltage confine the ions axially, and the RF field confines the ions radially in the following way. The two RF rods create a quadrupolar

potential, where the z axis is along the axis of the trap and the x and y axes are defined in figure 2-1. If we take this quadrupolar potential and insert it into Laplace's equation,

$$\Phi_{RF}(x,y) = C(ax^2 + by^2) \tag{2.1}$$

$$\nabla^2[C(ax^2 + by^2)] = 0 \tag{2.2}$$

we find that $a = -b$, and therefore the potential is attractive along one axis and repulsive along the other. This means that the ions would only be confined along one axis, and would leak out of the trap along the other. This is where the RF comes in. If we rotate this potential at frequency Ω_T (where the T means "trap") the ion sees a radial potential

$$\Phi_{RF}(x,y,t) = \left(\frac{x^2 - y^2}{2r_0^2}\right) V_0 \cos\left(\Omega_T t\right) \tag{2.3}$$

where r_0 is the distance between the ion and the rods and V_0 is the amplitude of the RF. We can also bias the RF rods with a DC voltage. If we include the DC voltages on the RF rods and the endcaps, the full potential [Gho95, PLB$^+$06] is

$$\Phi(x,y,z,t) = \Phi_{RF}(x,y,z)\cos\left(\Omega_T\right) + \Phi_{DC}(x,y,z) \tag{2.4}$$

$$\Phi(x,y,z,t) = \left(\frac{x^2 - y^2}{2r_0^2}\right)(V_0\cos\left(\Omega_T t\right) + \Phi_{DC}(x,y,z) \tag{2.5}$$

where $\Phi_{DC}(x,y,z)$ simply represents the electrostatic potential provided by the endcap and rod bias voltages.

Following Ghosh [Gho95] and using a potential in the form of equation 2.4, we can write down the equations of motion for the ion in the x and y directions, time average them, and then extract the effective potential

$$\Psi_{sec}(x,y,z) = \frac{Q^2}{4m\Omega_T^2} \left|\nabla\Phi_{RF}(x,y,z)\right|^2 + Q\Phi_{DC}(x,y,z) \tag{2.6}$$

where Q is the charge of the ion, m is the mass of the ion, and Ω_T is the RF drive frequency [Gho95, PLB$^+$06]. The ion is now fully confined in our trap by this trapping

potential, known as the secular potential. This trapping potential can also be used to explain planar traps.

2.1.2 The planar trap

Imagine unfolding a 4-rod trap onto a plane as in figure 2-2. We end up with a ground plane in the center, an RF rail on either side of this ground plane, and another ground electrode on the other sides of the RF rails. In our traps, instead of biasing the RF rails to get axial confinement, we bias the outer "ground" electrodes which we refer to as "mid" electrodes. Figure 2-3 shows a top view of the trap with endcap and mid electrodes included. Figure 2-4 shows the trapping potential created by a planar trap with the geometry of figure 2-3.

The trapping potential in this planar trap can be altered by the presence of stray DC fields, which can be produced by charging of dielectrics near the trap site. Since fibers and the structures we used to integrate them are dielectric, charging may be an issue when we attempt to trap ions with our fiber optic integrated trap.

2.2 The ^{88}Sr$^+$ Ion

The ^{88}Sr$^+$ ion is a convenient choice for ion trapping quantum computation experiments because it has a single valence electron, which gives it a simple electronic structure. Another reason ^{88}Sr$^+$ is particularly nice is because all of the relevant electronic transitions have transition frequencies which can be produced by diode lasers. This section describes the electronic level structure of the ^{88}Sr$^+$ ion and the laser-ion interactions that we use.

2.2.1 Level Structure and Lasers

Since the ^{88}Sr$^+$ ion only has one valence electron, the energy level structure that is important to us is very simple. Figure 2-5 shows a partial ^{88}Sr$^+$ ion level structure with relevant transition wavelengths and lifetimes labeled. We have lasers to address
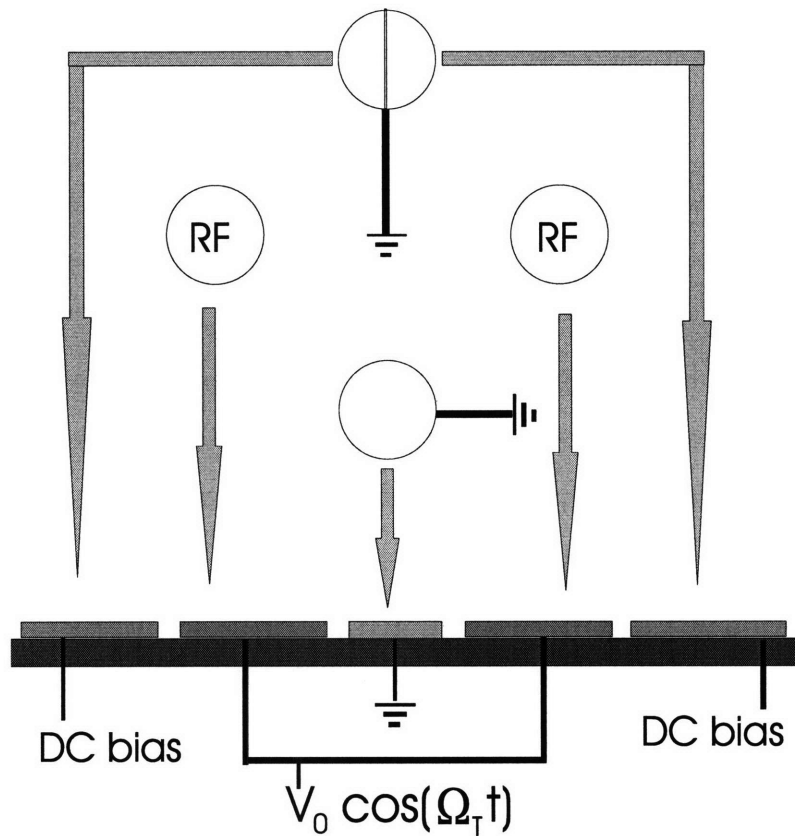
Figure 2-2: 4-rod trap unfolded into a planar trap. Blue is ground, orange is RF and green is DC biased "mid" electrodes. Drawing is not to scale.

4 of the transitions shown in the level diagram: 422nm, 674nm, 1033nm, and 1092nm. We also have lasers at 405nm and 460nm to photoionize neutral strontium.

The 422nm laser is used both for detection and Doppler cooling of the ion. When a ^{88}Sr$^+$ ion is in $5^2S_{1/2}$ (ground) state and is irradiated by 422nm light, the ion cycles between the $5^2S_{1/2}$ state and the $5^2P_{1/2}$ state. Since the lifetime of the $5^2P_{1/2}$ state is only 7.9ns, it decays quickly back to the ground state and emits a 422nm photon. If we continuously irradiate the ion with the 422nm light the ion will scatter photons in
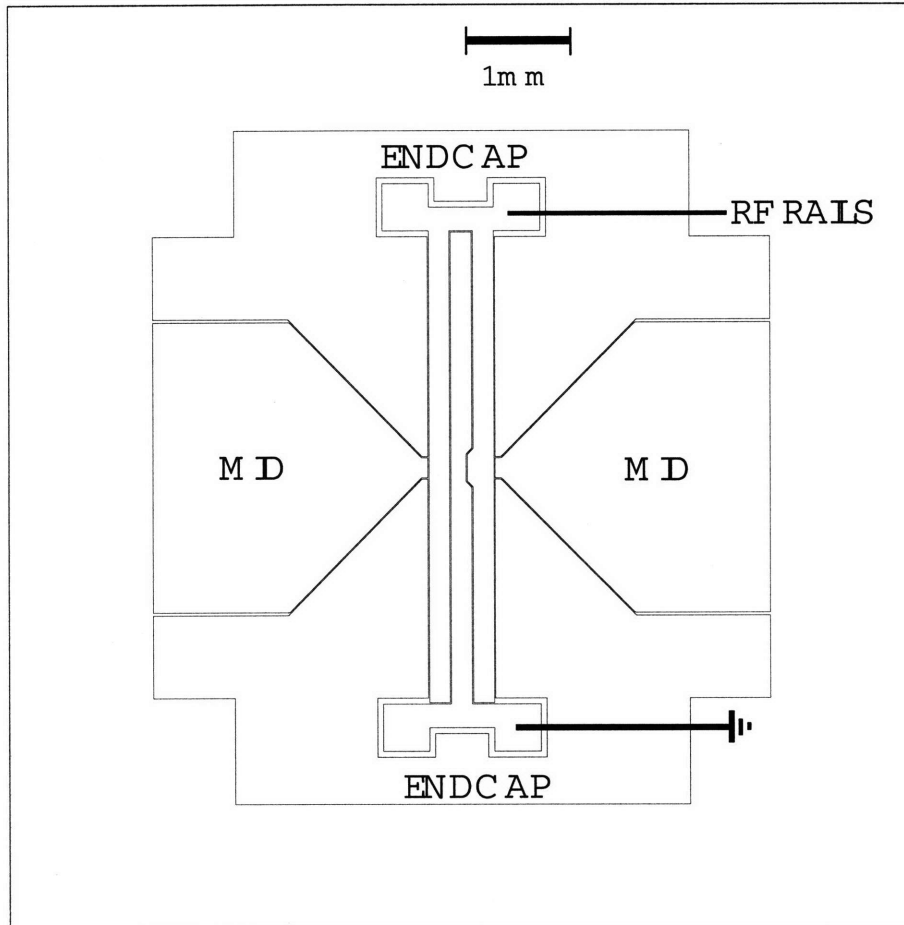
Figure 2-3: Planar trap. This is the actual trap geometry we use.
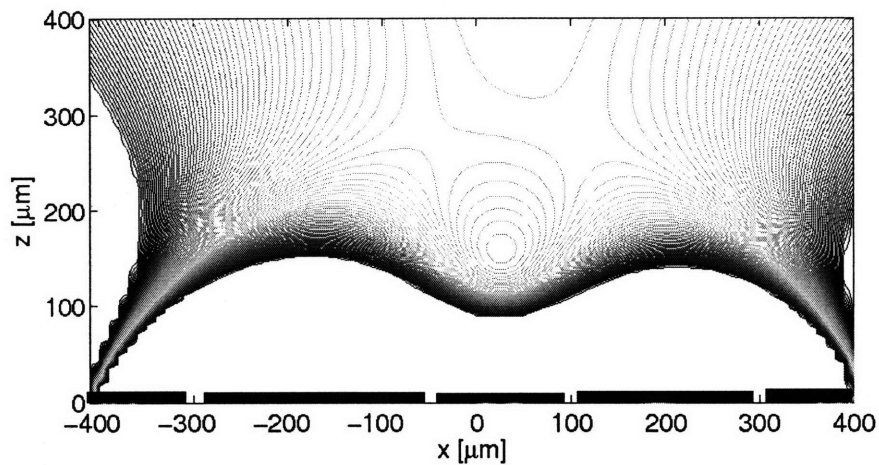
Figure 2-4: Computed secular potential in the x-z plane at the trap center of a 150μm trap for typical operating voltages. Isosurfaces are separated by 50 mV. Reproduced with permission from Labaziewicz et al [LGA+08].
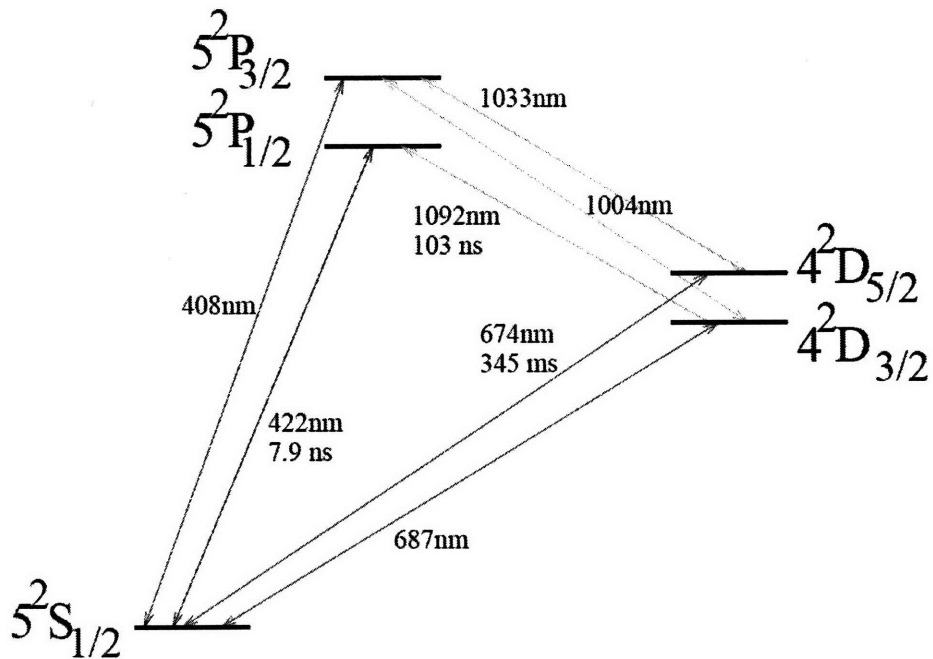
Figure 2-5: Partial energy level structure of ^{88}Sr$^+$ ion. Reproduced with permission from Richerme [Ric05].

this manner and we can detect the ion's fluorescence signal. We call the ground state the "light" state because of this fluorescence signal, and the $4^2D_{5/2}$ state a "dark" state.

When the ion is in the $5^2P_{1/2}$ state, it can also decay to the $4^2D_{3/2}$ state, which is fairly stable. If we simply allowed this to happen, after a short while all of the ions would be in the $4^2D_{3/2}$ state. We call this process shelving. In order to avoid shelving, we use the 1092nm laser, which re-pumps the ion back to the $5^2P_{1/2}$ state, where it can decay to the ground state and continue to cycle on the 422nm transition.

The 674nm laser is used for several things. The 674nm laser is used in conjunction with the 1033nm laser for sideband cooling, which is discussed in section 2.2.3. It is also used for addressing the $5^2S_{1/2}$ to $4^2D_{5/2}$ transition, which we use as an optical qubit, and temperature measurement.

2.2.2 Doppler Cooling

In addition to being the method of readout for the state of the ^{88}Sr$^+$, the 422nm line is used for Doppler cooling. We need to Doppler cool our ions in order to trap them. Doppler cooling works by detuning the 422nm laser to a lower frequency than the transition frequency such that an ^{88}Sr$^+$ ion moving into the laser beam will see a higher frequency (the frequency of the transition) via the Doppler effect, and will hence be on resonance and absorb the photon of lower frequency light. This gives the ion an amount of momentum in the direction parallel to the laser equal to $\hbar k$, where k is the wavevector of the incident light. The ion then emits a photon on resonance with the transition in a random direction. Averaged over many events, the ions will lose an average momentum of $\hbar k$ along the direction parallel to the laser, or an average energy of $\hbar(\omega_0 - \omega)$ where ω is the detuned frequency and ω_0 is the resonance frequency.

2.2.3 Sideband Cooling

We use the 674nm and 1033nm lasers for sideband cooling of our ions to their motional ground-states. We need to sideband cool our ions to achieve the stability required to perform coherent operations. Imagine an ion in the Nth motional state and the electronic ground state. If we excite the ion to the $5^2D_{5/2}$ state using a laser detuned by the secular frequency of the ion trap, the ion will then be in the $5^2D_{5/2}$ electronic state and the (N-1)th motional state. We then pump the ion up to the $5^2P_{3/2}$ state where it decays back to the ground state. We then repeat this process until the ion ends up in the motional ground state as well as the electronic ground state. We pump to the $5^2P_{3/2}$ state with the 1033nm laser because the lifetime of the $5^2P_{5/2}$ state is so long that sideband cooling would take forever if we did not pump to a state with a shorter lifetime [DBIW89].

2.2.4 Coherent Operations

Though coherent operations are beyond the scope of this thesis, they deserve mention because they are required to form quantum logic gates with trapped ions. Once we have an ion cooled to the motional ground state, we can do all sorts of interesting things with it. If we irradiate the ions with pulses of 674nm light of precisely controlled duration and phase, we can perform arbitrary rotations on the Bloch sphere and hence perform arbitrary unitary operations. For more information, see Ruth Shewmon's thesis [She08].

When performing these coherent operations on our trapped ions, it typically takes 1 ms to sideband cool the ion, between 4 and 100 μs to perform the operation, and 250μs to do the measurement. The speed of the entire operation could be significantly increased by increasing the measurement speed, which is the topic of section 2.2.5.

2.2.5 Detection and Measurement

In order to measure what a trapped ion is doing, we have to be able to collect the light that is scattered from the ion. In particular, we have to be able to distinguish whether the ion is in the $4^2D_{5/2}$ (dark) or $5^2S_{1/2}$ (light) state.

As described in section 2.2.1, when the ion is in the ground state, it will scatter 422nm light via the $5^2S_{1/2} \rightarrow 5^2P_{1/2}$ transition. When the ion is not in the ground state (for qubits we use the $4^2D_{5/2}$ state) it does not scatter any 422nm light. Given that photon scattering is a Poisson process, how many photons do we need to detect to be statistically certain that we have detected an ion in the ground state? Looked at another way, how long do we need to integrate for to be certain that detecting zero photons means that the ion is not in the ground state? For a Poisson process, if the expected number of photons arriving in a given time interval is N then the probability of there being exactly k photons arriving in this time interval is given by

$$p(N; k) = \frac{N^k e^{-N}}{k!}.$$
(2.7)

If we are looking to determine whether we have an ion in the dark state, we wish

there to be $k = 0$ photons detected. If we integrate for long enough that the we expect there to be $N = 4$ photons on average in that time interval, there is a 1.8% chance that if we detect zero photons it means that there is still an ion there that is in the ground state and is fluorescing. For our experiments, we typically integrate for a period of time that we would expect there to be $N = 12$ photons. This means that if we detect zero photons, there is only a $e^{-12} = .0006\%$ chance that the ion is in the ground state.

If we were able to gather all of the scattered photons, we could make measurements in a time $\tau = N/\sigma$ where σ is the scattering rate. When we illuminate a ^{88}Sr^{+} ion with our 422nm laser while it is in the ground state, it scatters about 10 million photons/s of 422nm light, depending on the laser power and detuning. In the case of $\sigma = 10^7$ photons/s, the time required per measurement would be 1.2μs. However, we cannot collect all of the photons scattered by the ion; we are limited by the solid angle and efficiency of our collection optics and PMT. With these modifications, the time required per measurement becomes

$$\tau = \frac{N}{\sigma}\left(\rho\eta\frac{\Omega}{4\pi}\right)^{-1}. \tag{2.8}$$

where Ω is the solid angle of collection of the imaging optics, η is the efficiency of these optics, and ρ is the efficiency of the PMT. Because of this, our experiments typically use a measurement time of 250μs. For typical values of parameters in equation 2.8 ($\rho = .2$, $\eta = .7$, $\Omega = .4$, $\sigma = 10^7$ photons/s, and $N = 12$), $\tau = 270\mu$s, which is approximately the measurement time we use. Increasing the speed with which measurements can be taken is of great interest to the quantum computation community, and can be accomplished by means of better light collection optics. η can be only marginally improved, ρ is expensive and difficult to increase, σ is inherent to the ion, and N is fixed by the low probability of mismeasurement we desire. It is Ω that can be improved the most by moving to a system with better light collection optics.

Chapter 3

Optics

The optics used to collect light scattered from the ions play an important role in the speed with which we can perform measurements of the electronic state of the ion, as discussed in section 2.2.5. This chapter introduces the traditional approach to collection optics in section section 3.1.1, and will discuss an alternative: fiber optics. Section 3.1.2 describes how fiber optics work, section 3.2 describes integration of fiber optics onto planar ion traps, and 3.2.1 describes the advantages of using fiber optics as a method of light collection.

3.1 Collection Optics

3.1.1 Current Optics

The current optics in the cryostat we use to collect scattered light consist of a high NA (numerical aperture) lens which is situated directly over the ion trap and other collimating and focusing lenses. This results in a high solid angle of collection (about .66 in our setup), but there are a few drawbacks. The first is that this imaging system is not very efficient. Not only do the photons have to go through several lenses, but there are also several windows to between the ion trap and the outside world as well as a few steering mirrors before the light finally makes it to the PMT. The second disadvantage of the current optics is that the imaging system is bulky. If

we were trying to scale the ion trap system to measure many ions at once, it would quickly become unmanageably large. The third disadvantage is that there is no way to distinguish between ions at different sites on the ion trap based only on the number of photons/s received. The advantage of the current optics is that we can also take a picture of the trap surface using a CCD, which aids in alignment of lasers and initial identification of ions when setting up the ion trap. Figure 3-1 is a schematic of the current optics setup.
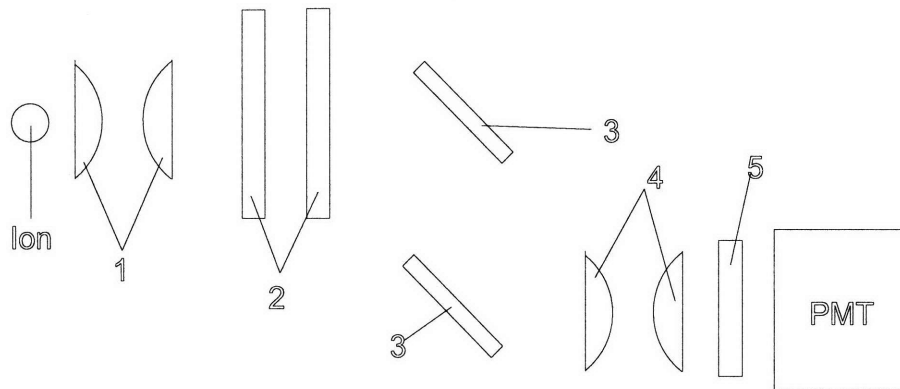

Figure 3-1: Standard collection optics in our cryostat. Photons are scattered by the ion on the left and then travel through the optics. (1) is a high NA lens and a focusing lens. (2) are the windows in the 77K shield and the vacuum shield. (3) are steering mirrors. (4) are focusing lenses. (5) is a 422nm bandpass filter. Finally, the photons enter the PMT and are counted. This diagram is not to scale.

The efficiency of the light collection optics depends on two things. It depends on the losses inherent to light interacting with surfaces, and also on the solid angle of collection of the optics. Some light is reflected at every surface the photons pass through, and the mirrors are not perfectly reflective. Table 3.1 tabulates these losses in the optics. Note that in our actual setup, there is also a beam splitter to send 30% of the light to a camera. However, this is not included in the losses because we want to compare collection power of the regular optics vs. fiber optics for light going directly to a PMT. It is important to note that these losses pale in comparison to the real issue with bulk optics: solid angle of collection, which is not included in this table

and is considered separately. Equation 2.8 says that the measurement time required depends on the product of $\frac{\Omega}{4\pi}$ and η where Ω is the solid angle of collection and η is the efficiency of the optics. Typical values of Ω in bulk optics are .1-.4, which give values of $\frac{\Omega}{4\pi}$ of .007-.03. This gives a total light collection efficiency on the order of 1%! Our imaging optics are better than most, with $\Omega = .66$ and $\frac{\Omega}{4\pi} = .05$. Clearly if the solid angle of collection can be improved upon, collection optics could be much more efficient.

Table 3.1: Efficiency of traditional collection optics. Note this does not include the solid angle of collection (Ω), which is extremely important and considered separately. The losses come from the data sheets for each optical element.

Optics	Losses	Efficiency	Number	(η) Total Efficiency
Mirrors	imperfect reflection	.98	2	.96
Lenses (AR coated)	reflections	.98	4	.92
Window (AR coated)	reflections	.96	1	.96
Window (uncoated)	reflections	.92	1	.92
422nm filter	reflections	.94	1	.94
(η) Total Efficiency				.73

3.1.2 Fiber Optics

Another option for collecting light scattered from ions is using fiber optics. Multimode optical fibers have a core made of glass which is coated by a cladding with a lower index of refraction, such that if the light enters the fiber at greater than the critical angle, the light will experience total internal reflection when it hits the interface between the core and the cladding. If you have two media where n_1 is the index of refraction of the medium the light is propagating through (in this case the fiber core) and n_2 is the index of refraction of the medium on the other side of the interface (in this case the cladding), and $\theta = 0$ is perpendicular to the interface, the condition for

total internal reflection given by Snell's law is

$$\theta \geq \theta_c = \arcsin\left(\frac{n_2}{n_1}\right) \tag{3.1}$$

where θ_c is the critical angle for total internal reflection.

Because of the requirement for total internal reflection, light can only propagate through an optical fiber if it enters from an angle less than the acceptance angle of the fiber. Snell's law at the fiber-core interface gives

$$n \sin \theta_{max} = n_1 \sin\left(\frac{\pi}{2} - \theta_c\right). \tag{3.2}$$

where $\theta = 0$ when light enters the fiber parallel to the core, θ_{max} is the maximum acceptance angle of the fiber, n is the index of refraction of air, n_1 is the index of refraction of the core. Figure 3-2 is a diagram of an optical fiber with the maximum light acceptance angle and total internal reflection [GT98].
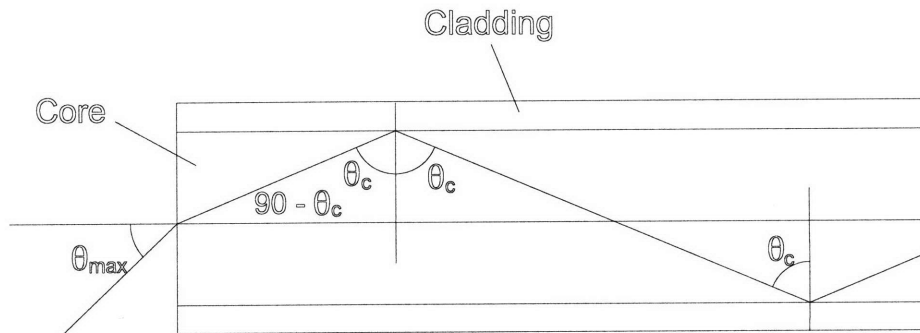
Figure 3-2: Optical fiber with maximum light acceptance angle (θ_{max}) and the critical angle for total internal reflection (θ_c). This diagram is not to scale.

Fiber optics have a specific numerical aperture (NA) that is inherent to the fiber and depends on the indexes of refraction of the core and cladding. Fiber optics are sold with their NA specified, not the indexes of refraction of the core and cladding. It is therefore useful to transform our equations so they contain only the NA of the

fiber instead of the indexes of refraction of the core and cladding. If we substitute equation 3.1 into equation 3.2 and apply some trigonometric tricks, we find that the NA is given by

$$n \sin\left(\theta_{max}\right) = \sqrt{n_1^2 - n_2^2} = NA. \tag{3.3}$$

The optical fiber we used for this experiment was a step-index multimode fiber with a 200μm core and a NA of .22.

If we are attempting to collect light scattered from an ion with fiber optics, the NA of the fiber plays an important role in determining how much of the scattered light we can collect. If it wasn't for the NA of the fiber, the closer we placed the ion to the fiber tip, the larger the solid angle of collection there would be. However, because there is a limited acceptance angle, at some point bringing the ion closer to the fiber will not increase the solid angle of collection. The maximum distance d between the fiber and the ion for the largest possible solid angle of detection is given by

$$d = \frac{D}{2}\tan\left(\frac{\pi}{2} - \theta_{max}\right) \tag{3.4}$$

$$d = \frac{D}{2}\cot\left(\arcsin\frac{NA}{n}\right) \tag{3.5}$$

$$d = \frac{D}{2}\frac{\sqrt{1 - \left(\frac{NA}{n}\right)^2}}{\frac{NA}{n}} \tag{3.6}$$

where D is the diameter of the fiber core and n is the index of refraction of air. Plugging in the core diameter and NA of our fiber, we find that the maximum distance the ion can be from the fiber tip before we start losing solid angle is 443μm. This would correspond to a solid angle of collection of .15.

3.2 Integration of Fiber Optics On Planar Traps

Now that we know a bit about how fiber optics can collect light, we can think about how to integrate them onto planar ion traps. Since fibers are made of dielectric, which can collect charge, it is best to keep them as far away from the ion as possible. If too much charge gathers near the ion trap potential, the resulting electric field can

deform the potential enough so that it will no longer trap ions. However, we also want the fiber to collect as much of the scattered light as possible. Therefore, it is best to design the fiber integration scheme such that the fiber is at the maximum distance from the ion before the solid angle drops off dictated by equation 3.6.

The fiber-ion distance we actually used is about 650μm. The reason for this is because we had to make sure that the fiber was both out of the way of the lasers, and also not on top of the RF electrodes. Section 4.1.2 describes the alignment structures we used and to hold the fiber in place on the trap and the process we used to fabricate them.

3.2.1   The Advantages of Fiber Optics

Fiber optics offer several advantages over traditional optics. First of all, they are much smaller. In principle, the bulky many-component imaging optics can be replaced by a fiber, a 422nm filter, and a PMT. In reality, since we are operating in a cryostat we also have to have a convenient way of getting a fiber from inside the cryostat to the PMT outside. Section 5.1 describes the fiber feed-through we constructed for this purpose. Figure 3-3 shows the optical path of a photon scattered from an ion and then being detected via fiber optics. Table 3.2 tabulates the losses in the fiber optic detection system. Note that solid angle of collection is not included in this table and is considered separately. The efficiency of fiber collection optics are similar to those in the traditional imaging optics, which make them a viable option for light collection. The important question is then what the solid angle of collection of the fiber is. The fiber we used has a maximum solid angle of collection of .15, which is comparable to typical values for traditional optics.

With the fiber at a distance of 650 μm from the ion, our collection efficiency was only .6%, but if we had used a higher NA fiber, we could get higher photon detection efficiency. We could easily buy fibers with a NA up to .48, and the NA of optical fibers can be increased even more by lensing the ends of the fibers. To give an idea of the numbers, a fiber with a 200 μm core and an NA of .5 gives a solid angle of collection of .83, which corresponds to a value for $\frac{\Omega}{4\pi}$ of 6.6%. Fiber optic collection
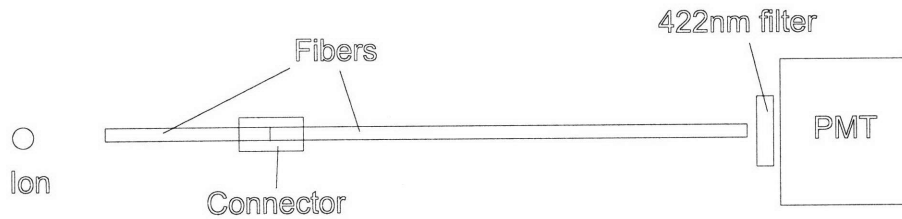
Figure 3-3: Optical path of light scattered from photon and detected by a fiber.

Table 3.2: Efficiency of fiber collection optics. Note this does not include the solid angle of collection (Ω), which is extremely important and considered separately. The losses come from the data sheet for each optical element.

Optics	Losses	Efficiency	Number	(η) Total Efficiency
Fiber-Air interface	reflections	.96	2	.92
Connector sleeve	reflections, imperfect alignment	$\leq$.90	1	$\leq$.90
422nm filter	reflections	.94	1	.94
(η) Total Efficiency				.78

can offer a slight advantage for overall light collection efficiency.

Another advantage of fiber optics is that because the optical fibers are so much smaller than the traditional optics, it is possible to put many of them on the same ion trap. This could be used for two different purposes. The first is to have many fibers collecting light from one ion, and thereby further increasing the solid angle of detection. The second is to have different fibers pointing at different sites on an ion trap. Because each fiber has a maximum light acceptance angle, as long as the ions were situated so as to only be in the light acceptance cone of one fiber, we would be able to distinguish between and measure several different ions simultaneously. Chapter 7 describes one scheme for implementing multiple fibers on a multi-site ion trap.

Chapter 4

Fabrication

Just like classical computers, as quantum computers scale to larger numbers of qubits, the individual qubits will need to take up less room. One of the more promising ways to achieve a scalable quantum computer is by using microfabricated planar ion traps. A constant fraction of all the ions in these traps will need to have sites with ion detection optics, which can be scaled to smaller sizes by integrating fiber light collection optics onto these planar ion traps [KK07].

This chapter discusses the microfabrication techniques required to fabricate a planar ion trap (section 4.1.1) and fiber mounting structures (section 4.1.2), as well as the specific process used for fabrication. Section 4.2 presents the process for integrating a multimode fiber onto the completed ion trap.

4.1 Microfabrication Techniques

4.1.1 Trap Fabrication

Microfabrication is the process of fabricating micrometer scale devices such as semiconductor devices, microelectromechanical systems, and integrated circuits. Microfabrication is more of an art than it is a science. If the humidity or temperature in the room is slightly different than normal, a process might completely fail. Knowing how to deal with potential problems like these takes years of practice. Luckily, our lab has

been making ion traps for years now, and we have an expert. Yufei Ge fabricated the trap for my project using the process described in this section.

For this experiment we used a microfabricated planar trap of gold on quartz. The trap design we used is the same as the trap discussed in section 2.1.2. The trap was designed to have an ion height of 130μm to align it with the axis of the 260μm diameter optical fiber we intended to put on the surface of the trap.

A standard technique in microfabrication is photolithography, which is a process by which a pattern can be transferred from a photo-mask to a wafer by means of a UV-sensitive chemical called photoresist. Before we began microfabrication, we had to draw up a photo-mask for each layer of features that we wished to be on our final trap. For the first layer, we drew up our trap design in Autocad (see figure 4-1) and sent it out to Advanced Reproductions Corporation to be turned into a mask. Note the crosses on the corners of the trap. The reason for the crosses is so that we could coalign the structures which hold the fiber and the trap structures.
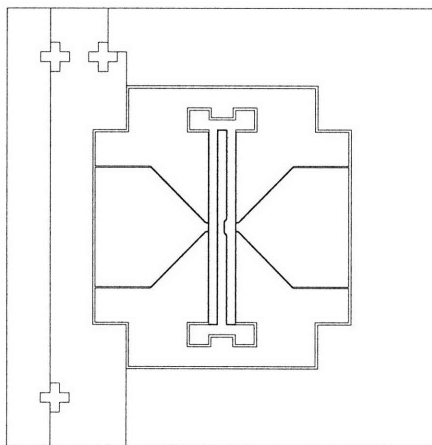

Figure 4-1: Design for ion trap, the trap is 1cm across. The crosses are for alignment.

The first step in fabrication is preparing the wafer. The wafer we used is a 1cm by 1cm square of single crystal quartz with a $75\mathring{A}$ layer of titanium on top, and a

.05 μm layer of silver on top of that. The purpose of these layers is to get the gold to bond to the quartz. The titanium bonds well to quartz and silver, and the silver bonds well to gold and titanium. To prepare the wafer, we baked it at 120C on a hot-plate for 5 minutes to boil off impurities.

Next, we put positive photoresist onto the surface of the wafer. Positive photoresist is a material which when baked will form cross-links and will harden into an epoxy-like substance. If you expose the positive photoresist to UV light after baking, the cross-links break and the material can be washed away with a solvent. We used AZ 4620 photoresist and applied it by putting about a ml on the wafer and spinning the wafer at 2500 RPM for 10 seconds, and then 4500 RPM for 60 seconds. Spinning at these speeds gives a very thin even coat of photoresist on the surface of the trap. After spinning, we baked in an oven at 90C for 5 minutes to solidify the photoresist.

The next step is to expose the wafer to a pattern of UV light. The light source is a 200W mercury lamp with filters for 365 and 405 nm. The pattern is created by a mask of chromium on glass that is created from our trap design. The mask has chromium everywhere where we wish to have photoresist on the wafer, and is clear everywhere where we want to wash the photoresist away. We exposed the wafer 3 times for 7.5 seconds at an interval of 30 seconds. The reason for exposing multiple times for a short period of time is to reduce stresses that build up in the photoresist upon exposing.

After exposing, we developed the trap in a developer called AZ 440 MIF, sourced by the AZ Electronic Materials Co., for 5 minutes. This washed away all of the photoresist in the areas where we wished there to be electrodes, and left small strips of photoresist between the electrodes. These strips were 10 μm wide on the mask, but shrunk to 6 μm wide after processing. Next, we gold-plated the wafer. The gold sticks to everywhere the wafer is exposed, but not where the photoresist is. We electro-plated with Transene TSG-250 plating solution at 70C for 20 minutes with a stirring speed of 300 RPM and a current of 10 mA to get a gold thickness of about 5μm.

At this point, there is silver and titanium both underneath and between the elec-

trodes. To keep the electrodes from shorting to each other, we have to remove the silver and titanium from between the electrodes and leave only single crystal quartz. After removing the wafer from the electro-plating bath, we rinsed with acetone and isopropyl alcohol. Next, we etched away the silver from between the electrodes by placing in a bath of $NH_4OH:H_2O_2:H_2O$ (1:1:4) for 15 seconds. Then we etched the titanium by placing the wafer in a bath of $HF:H_2O$ (1:2) for 15 seconds. After rinsing off the etching solution, the trap is finished. Figure 4-2 is a picture of a finished trap.
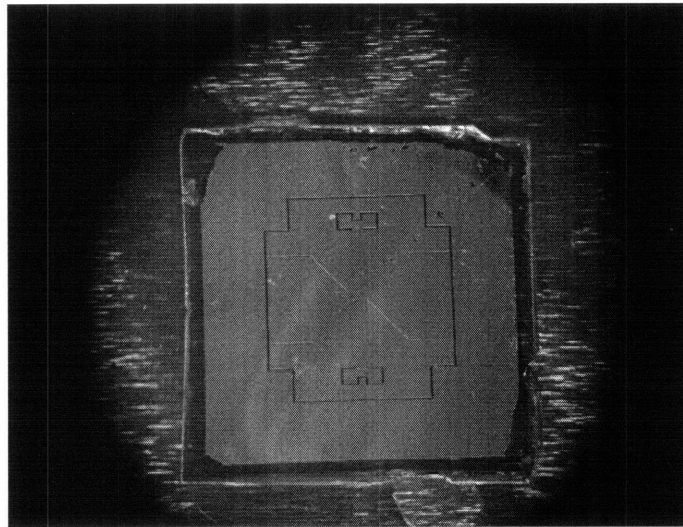

Figure 4-2: Finished gold on quartz trap. There are no alignment crosses on this trap because it was made in a previous batch. The quartz square is 1cm x 1cm.

4.1.2 SU-8 Alignment Structures

After fabricating our ion trap, we need to add alignment structures for the fiber optic that we want to integrate on the trap. The purpose of these alignment structures is two-fold. The first is to physically hold the fiber on the trap, and the second is to align the fiber to the trap structures so the fiber tip will be in the best position to view the ion. The specific numbers for the optical fiber on this ion trap are discussed in section 3.1.2. Figure 4-3 shows the design for our alignment structures, which was adapted from the design used in Liu's "Fabrication of alignment structures for a fiber resonator using deep ultraviolet lithography" [L+05]. I did all of the fabrication in this section, with advice from Yufei Ge.
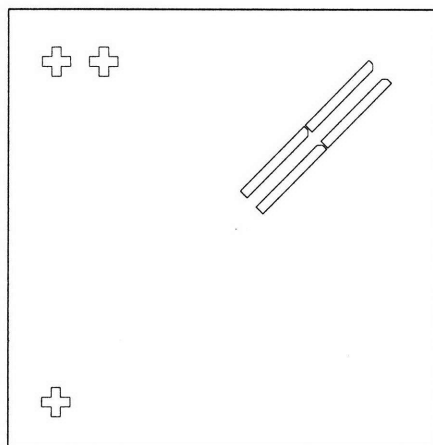
Figure 4-3: Design for fiber alignment structures. Each rectangular structure is 1000μm long and 200μm wide. The crosses are for aligning the mask to the trap.

Before fabricating fiber alignment structures on our ion trap, we fist did extensive testing of the fabrication process described in this section. We tested several different photo-resists for creating fiber alignment structures such as SU-8 2050, SU-8 2100, and SU-8 3050. These mostly differ in viscosity and adhesion properties. We also tried various exposure times and channel widths, as features tend to expand or shrink compared to the mask size with different exposure lengths. After many test runs, we finally settled on the process that is described in this section. Figure 4-4 shows one of the preliminary fiber alignment structures. Figure 4-5 shows a cross section of one of the test fibers which was 125 μm in diameter in the fiber alignment structures.

To create alignment structures, we used SU-8 2100. This is a negative photoresist which hardens into an epoxy-like substance. Negative photoresist works exactly opposite of how positive photoresist works. When you expose negative photoresist to UV light, it creates cross-links in the photoresist. Then, the parts of the resist that haven't been exposed to UV light can be washed away with solvent, leaving only the pattern that was exposed to UV light. SU-8 2100 is a good choice for permanent
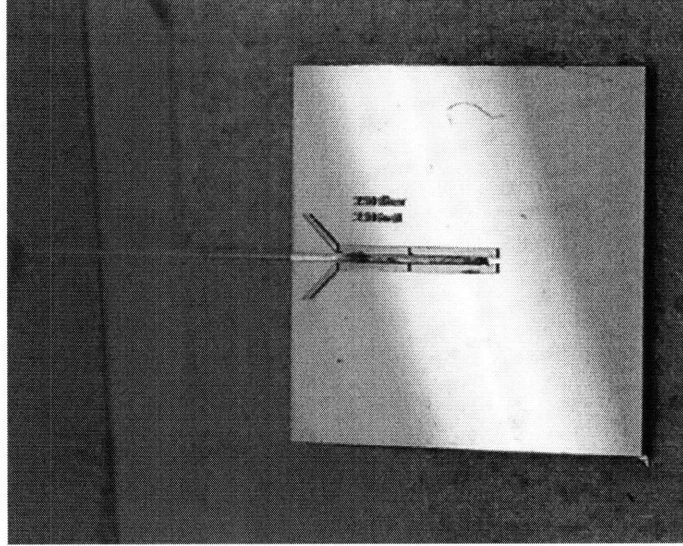
Figure 4-4: Test fiber alignment structures. The silicon square is 1cm x 1cm.

surface structures because it is extremely robust. The adhesion strength to glass is 35 mPa, and it is virtually impossible to remove by chemicals after it has been fully cured. It can also be applied in extremely thick coats and structures can be fabricated with a very high aspect ratio. SU-8 also has excellent thermal stability, which is important because we are using our trap in a cryostat.

We began by creating a mask from the design shown in figure 4-3. Note that the same crosses that are on the trap mask are also on this mask. This is so we can align the structures later. Next, we put SU-8 on top of the finished trap. However, SU-8 is very viscous, so placing it directly on the 1cm by 1cm trap didn't work very well. We solved this problem by attaching the trap to the center of a dummy wafer using a drop of NR7 (another type of photoresist). We then set the NR7 by baking on a hot-plate at 95C for 4 minutes. Next, we applied a few ml of SU-8 2100 to the trap and wafer and spun it at 1000RPM for 10 seconds, 2500RPM for 30s, and 700RPM for 10s. This gave a resist thickness of about 170μm, which is sufficient to hold down our fiber. (Since the fiber diameter is 260 μm, we need resist slightly thicker than half the diameter to hold the fiber.) To set the resist, we baked on a hot-plate at 65C for 7 minutes and then 95C for 45 minutes.

After applying the resist, we aligned the fiber alignment structure mask to the finished trap using a Karl Suss mask aligner. We accomplished this by taping the
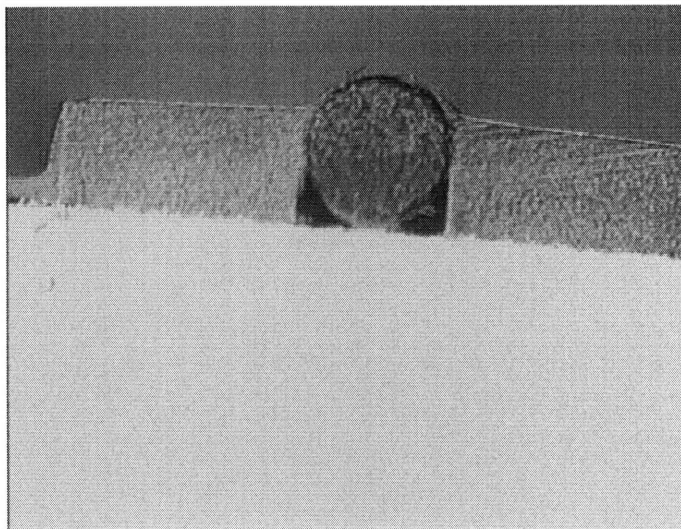
Figure 4-5: Cross section of SU-8 alignment structures with a fiber. The fiber diameter is 125μm.

wafer with the trap down to the chuck, and then slowly rotating and translating the wafer under the mask while looking at it through a microscope. When all three crosses on the mask were aligned with the crosses on the trap, the wafer was very carefully put into contact with the mask. Figure 4-6 shows a trap with SU-8 alignment crosses that have not been properly aligned. We then exposed the wafer with 365nm and 405nm light for 4 minutes. This is a slight over-exposure of the SU-8, which results in side-walls which are slightly over-vertical. This allows the SU-8 to grip the fiber and hold it flush again the trap surface. We then post exposure baked the wafer at 65C for 6 minutes and 95C for 17 minutes.

After baking, we developed the wafer in PM acetate (propylene glycol monomethyl ether acetate) for 5 minutes and then rinsed with isopropyl alcohol. We then dipped the wafer in acetone for 15 seconds to remove the trap from the wafer, and then rinsed in isopropyl alcohol again. Finally, we post-baked the trap at 95C for 3 minutes to firmly attach the SU-8 to the surface. We then let the trap sit for 3 days to allow the SU-8 to fully cure before attempting to insert the fiber. During process testing, we found that if the structures were mechanically loaded before sitting for a few days, the SU-8 structures would break off rather easily.
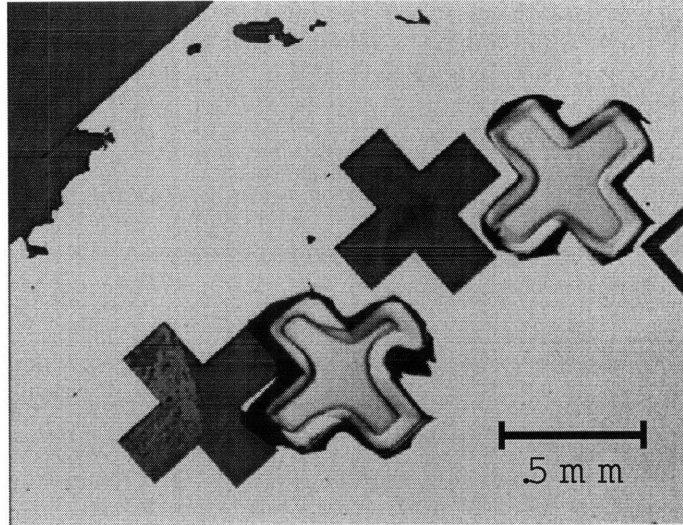
Figure 4-6: Alignment crosses on trap and in SU-8. These structures are not properly aligned. The darker crosses are on the trap, and the raised crosses are made of SU-8.

4.2 Trap Mounting and Attachment of Fiber

After all of the microfabrication was complete, the trap needed to be mounted to a CPGA (ceramic pin grid array) and wire-bonded so that we could apply voltages to the trap electrodes. Yufei glued the trap to a copper spacer on the CPGA and then wire-bonded the electrodes to the CPGA. After Yufei did the mounting and wire-bonding, I prepared a fiber for insertion into the alignment structures using the process described below.

First, we had to prepare a fiber for insertion into the trap. We used OZ optics step index multimode fiber (QMMF-UVVIS-200/240-0.4-L) which has a core diameter of 200μm, a cladding diameter (with hard coat) of 260μm, and a buffer diameter of .375mm. First, we stripped the buffer off of 20mm of both ends of the fiber. Then, we cleaved the ends of the fiber to get a nice flat surface. This is accomplished by taping the end of the fiber to the edge of the table, scoring the surface of the fiber perpendicular to the axis very lightly, and then pulling on the fiber along the axis.

Next, we connectorized one end of the fiber with a SMA connector using the basic process described in the Thorlabs Guide to Connectorization and Polishing Optical Fibers. Briefly, we filled the end of the connector with F112 epoxy until a bead formed on the surface, inserted the fiber, cured the epoxy, cleaved the end of the fiber

which was protruding past the epoxy bead, and then polished the fiber tip using and SMA polishing disk and 5μm polishing sheet, 3μm polishing sheet, and then finally 1μm polishing sheet. We did not add protective housing to the fiber. The result was a fiber with a SMA connector on one end and a flat cleaved surface on a stripped section of fiber on the other end.

Next, we inserted the fiber into the alignment structures very carefully, and slid the fiber forward until it was almost touching the RF rails. Then, we epoxied the fiber to the CPGA to keep the fiber from pulling out of the alignment structures during handling. Figure 4-7 shows the mounted trap with the fiber inserted into the alignment structures. Figure 4-8 shows more of the CPGA. Note the capacitors on the edges of the CPGA. These are to keep stray RF from running around.
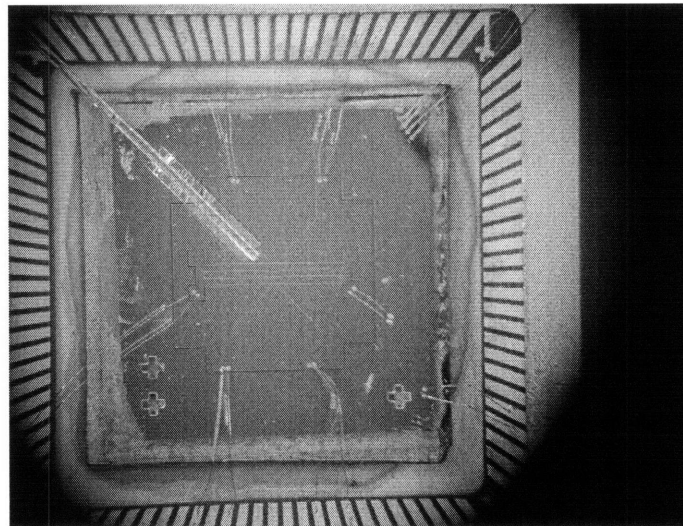

Figure 4-7: Finished ion trap mounted on CPGA with fiber inserted into alignment structures. The quartz square is 1cm x 1cm.
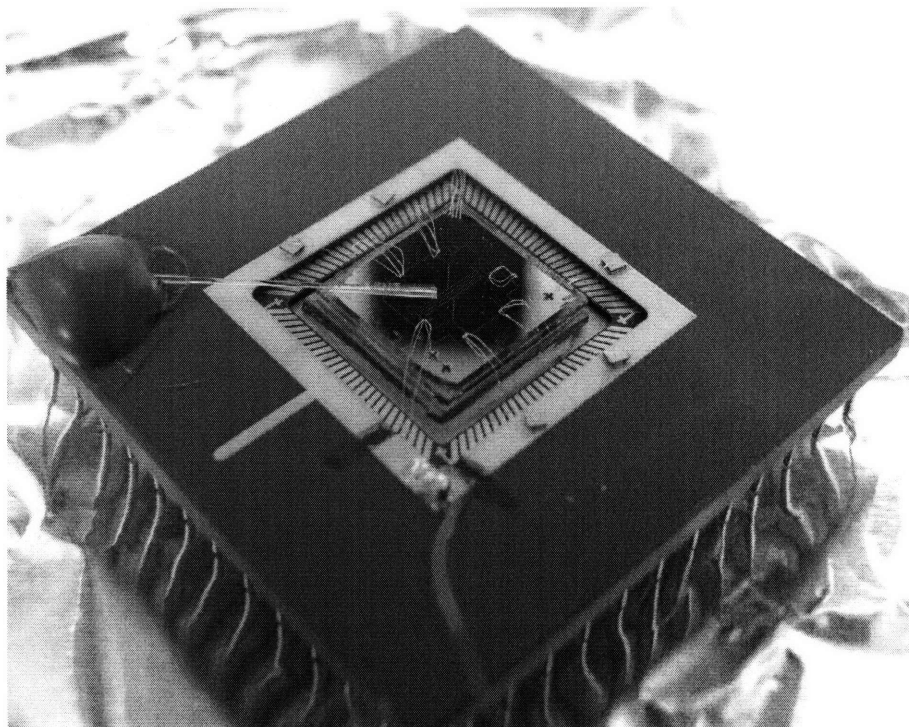
Figure 4-8: Wider view of finished ion trap on CPGA with fiber. The gold on quartz trap is 1cm x 1cm.

Chapter 5

Experimental Setup

Trapping ions requires a complicated experimental setup with three main components. The trap must be in a vacuum environment, there must be a source of ions, and there must be optical access for lasers. A vacuum environment is required because ions react quickly with any chemicals around them. A vacuum environment suitable for trapping can either be achieved by inserting the ion trap in an extremely clean UHV chamber, or by inserting the trap in a high vacuum cryostat and cooling down to low temperatures. Because we are using SU-8 epoxy which outgasses at UHV pressures, we decided to insert our ion trap into a cryostat at high vacuum pressures to do experiments. Section 5.1 describes how we integrated our fiber integrated ion trap into an existing cryostat setup. Jaroslaw Labaziewicz's thesis describes the existing cryostat setup in more detail [Lab08]. Section 5.2 describes how we trap ions once the trap is in the cryostat, including ion creation and lasers. Section 5.3 describes measurement of the fiber light collection ability.

5.1   Integration into Cryostat

After preparing the trap with the integrated fiber, we had to integrate the trap into the cryostat. Figure 5-1 shows a diagram of a cross-section of the cryostat. The reason we decided to do this experiment in a cryostat is because the buffer on fibers and SU-8 are both "soft" substances, which means that they outgas significantly at

low pressures. These substances are made of large enough molecules that at cryogenic temperatures they freeze out and no longer outgas.
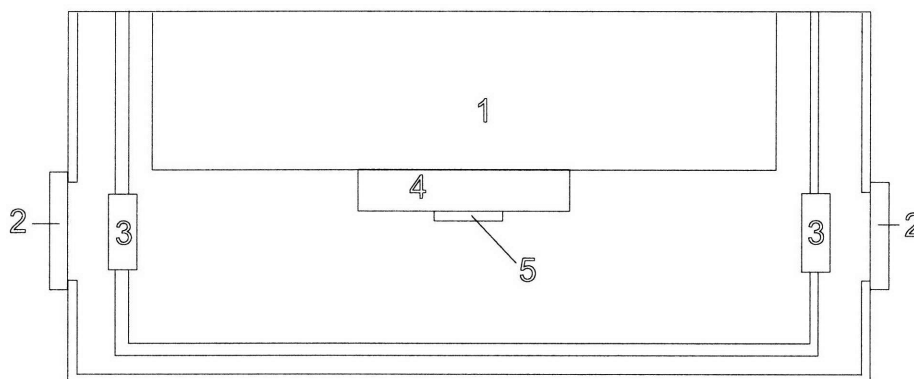

Figure 5-1: Simplified cross section of cryostat. (1) is the 4K shield. (2) are the vacuum windows (mounted on the vacuum shield). One of these gets replaced with the fiber feed-through. (3) are the heat filters (mounted on the 77K shield). One of these gets replaced with the heat filters with slots. (4) is the CPGA in the socket. (5) is the trap. This figure is not to scale.

The first challenge was getting the fiber through the vacuum window and into the cryostat. We accomplished this by replacing one of the 2" diameter windows with a 2" diameter disk of aluminum with a 1" window mounted in the center and sealed in place with torrseal, a low vapor-pressure epoxy resin sold by Varian, Inc. A hole was drilled through the aluminum disk and a fiber was fed through the hole and torrsealed in place. The end of the fiber inside of the cryostat was prepared in the same way as the connectorized end of the fiber attached to the ion trap, described in section 4.2. The end of the fiber outside of the cryostat was prepared in much the same way, except for the addition of a protective sheath over the fiber and a strain relief boot at the connector. Figure 5-2 is a diagram of the fiber vacuum feed-through. Figure 5-3 is a picture of the feed-through installed in the cryostat.

Our next task was getting the fiber through the 77K shield in the cryostat. In the 77K shield there are small windows and copper support pieces which hold the windows in place. These act as heat filters to keep the radiation from the room from leaking into the cryostat. In order to get the fiber through one of the heat filters, we made a new set of copper support pieces with a slot cut through them. This allowed us to insert the fiber through the 77K shield and then install the heat filter while
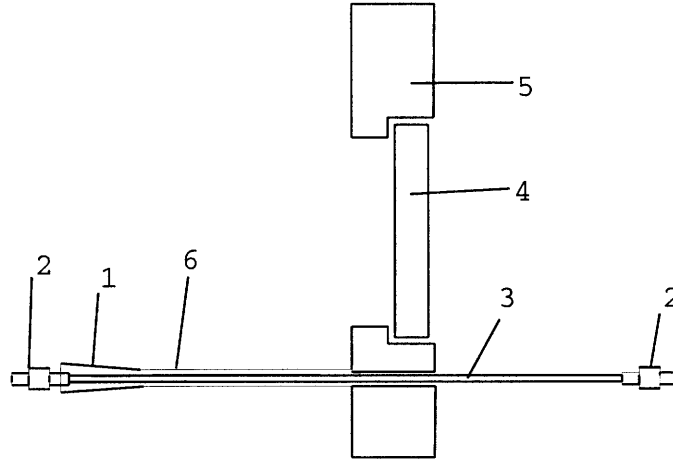
Figure 5-2: Digram of fiber vacuum feed-through. 1 is the strain relief boot. 2 are the SMA connectors. 3 is the fiber. 4 is the window. 5 is the aluminum disk. 6 is the protective sheath on the outside of the cryostat. This figure is not to scale.

carefully placing the fiber in the slot. Figure 5-4 shows the heat filter with the fiber going through the 77K shield.

At this point the fiber goes from outside the cryostat into the chamber which contains the trap. The only task which remains is connecting the fiber on the trap to the fiber from outside the cryostat. We made an L-shaped bracket which was screwed down to the 4K base-plate and held an all metal SMA-SMA connector about 2.25" above the 4K surface. This allowed all of the fibers to be above the optical plane of the lasers. Once the trap was installed in the CPGA socket and the fibers were plugged into the connectors, all that was left was placing the camera optics over the trap. Figure 5-5 shows the trap installed in the cryostat with connected fibers, and Figure 5-6 shows the same with the imaging optics placed over the trap.

Once we had everything installed in the cryostat, we closed it up and pumped it down with a turbo pumped by a roughing pump. At first there was a leak in the fiber feed-through, but we quickly found it and sealed it with torrseal. After the pressure dropped some, the first test we did was to shine laser light back through the fiber to see if it came out on the trap. Visual inspection of the inside of the cryostat showed that there was indeed light coming out of the fiber. Photos taken with the imaging optics with the laser on and off confirm this. Figure 5-7 shows the fiber with and without the laser on.

Figure 5-3: Fiber feed-through installed in cryostat. The glass window is 1" in diameter.

Once we confirmed that everything was working properly, we began preparing for trapping ions.

5.2 Cryostat Operation and Trapping Ions

Shannon Wang helped me install my traps and fibers in the cryostat and helped me with operation of the cryostat for trapping ions. I used our lab's standard procedure for operating the cryostat. The procedure we followed is documented briefly in this section.

Pumping down takes about 12 hours, and during this time we outgassed the activated charcoal getters (which are used when we are cold to absorb molecules) and the vacuum line between the cryostat and the turbo pump. When the pressure
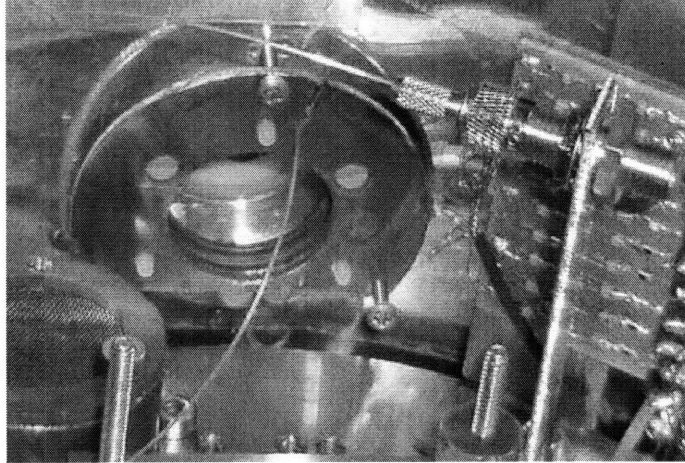
Figure 5-4: Heat filters (copper and glass, left side) with fiber coming through. The inner hole in the heat filter is 21.2mm. Fiber connector (right side, steel), 33mm long).

is around $2\text{-}3\cdot10^{-6}$ torr, the pressure is good enough to cool down. Right before we cool down, we outgas our strontium oven by turning the current up to 5A, letting the pressure rise, waiting until the pressure drops back to what it was before outgassing, and then turning off the oven. At this point, we fill the inner (He) and outer (N_2) tanks in the cryostat with liquid nitrogen and cool down.

Once we were cool, we aligned all of the lasers (422nm + 1092nm, PI (405nm + 460nm), and 674nm) to the trap surface by using the camera. At this point the pressure should be around $2\text{-}3\cdot10^{-7}$ torr. Then, we turned on the trap DC electrodes and RF to check for shorts. Then we scanned the RF frequency at 120mV to find the peak response. We started with DC voltage values of +10V on the endcaps, and -10V, -8V on the mid electrodes, and RF at 150mV at 34.7MHz. Once we determined that everything was working, we turned the oven up to 5A and began attempting to trap.

Trapping ions is extremely difficult because there is a very large parameter space to search. DC electrode voltage magnitude and relative values, RF voltage, 422nm laser alignment, and PI laser alignment are all important, and if any of them are wrong we will fail to trap. After several hours of attempting to trap and failing, we determined that the pressure in our cryostat may be to blame. At liquid nitrogen temperature, the pressure was $1.2\cdot10^{-6}$ torr, which was almost an order of magnitude
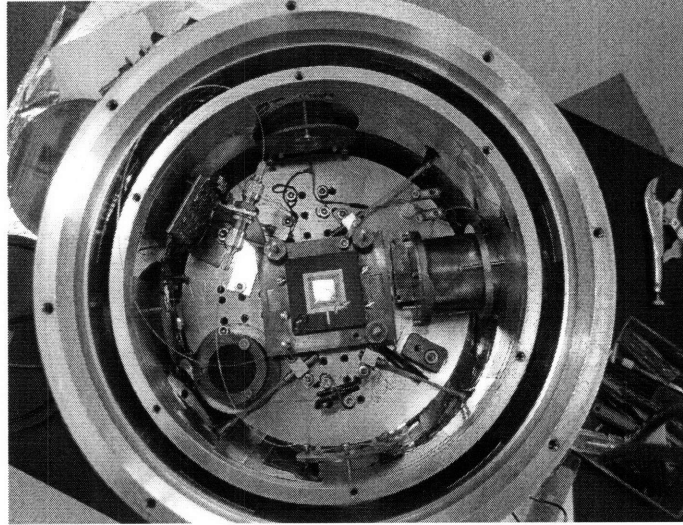
Figure 5-5: Trap installed in cryostat with fibers connected. The trap is 1cm x 1cm.
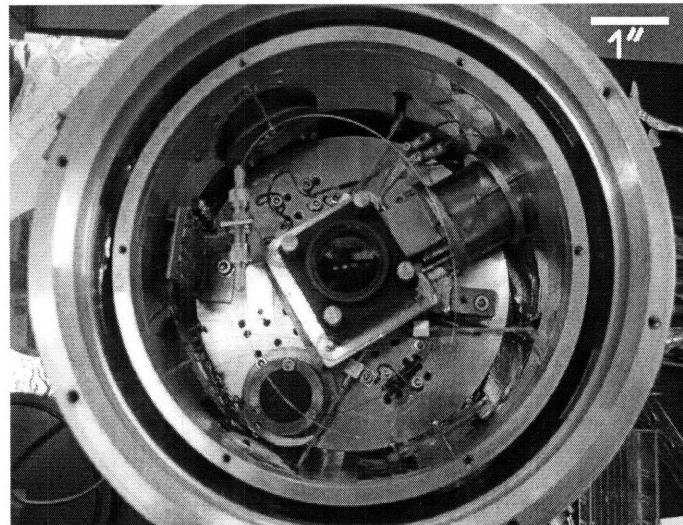

Figure 5-6: Trap installed in cryostat with fibers connected and camera optics installed.

above the pressure that we normally trap at. We also noticed that the pressure was fluctuating a lot, so we put Vacseal (high vacuum leak sealant) around the fiber in the fiber feed-through to seal any potential tiny leaks, and warmed up the cryostat. We decided to bake the cryostat at 60°C for a few days to try to evaporate any accumulated materials off the surfaces in the cryostat. We baked by running hot air through the nitrogen tank of the cryostat while pumping with the turbo. A plot of the pressure over several days of baking is shown in figure 5-8.

After baking and cooling down again, we achieved a pressure of $5.0 \cdot 10^{-8}$ torr.
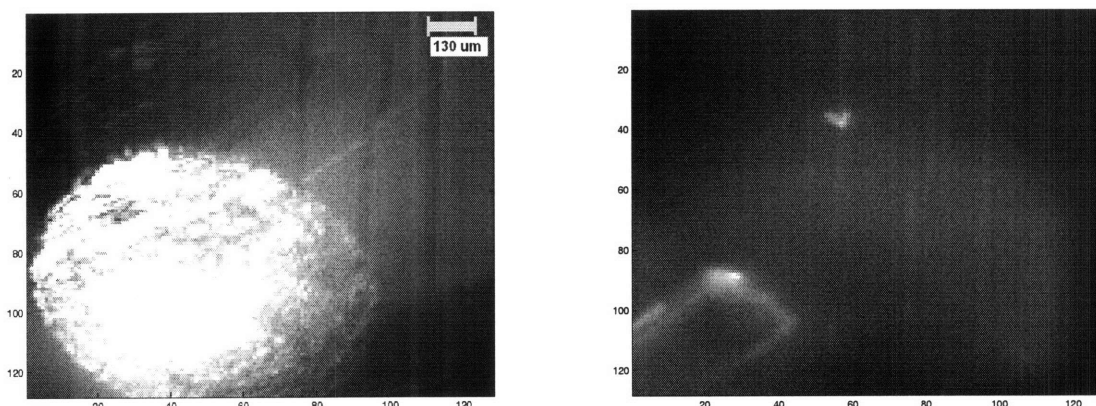
Figure 5-7: Fiber on trap with laser on (left) and off (right). The fiber can be seen in the lower left corner of the right image. The bright spot over the fiber tip on left image is scattered light. The scale on both photos is the same.
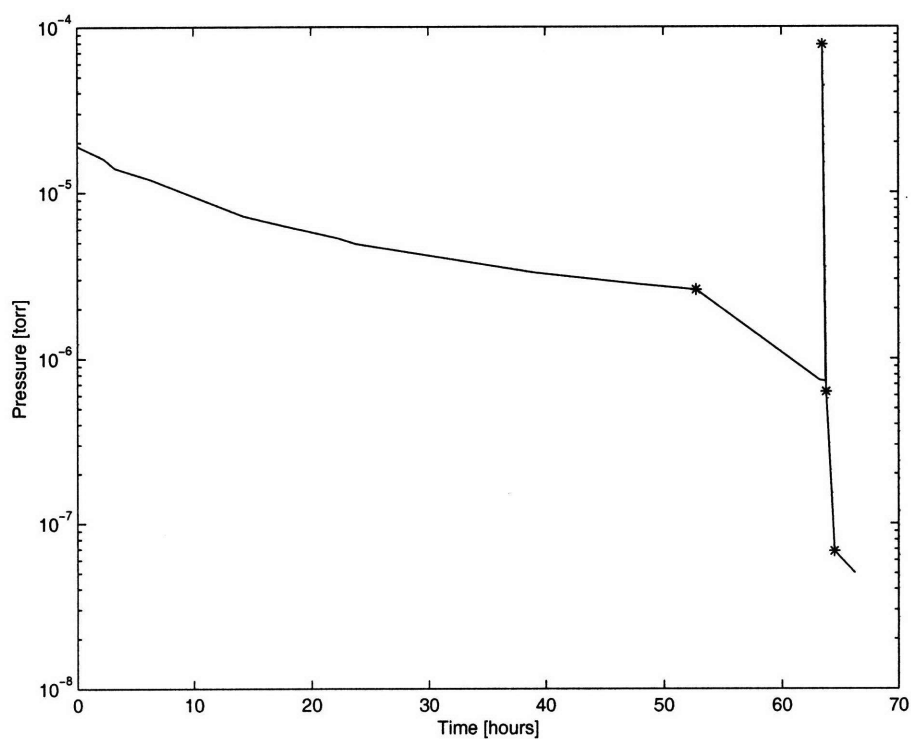
Figure 5-8: Pressure at the ion gauge in the cryostat during baking at 60°C. From left to right: the first star is turning the heaters off, the second star (peak) is outgassing the oven, the third star is the start of cooling down, and the last star is when we first reach 77K.

However, after several hours of scanning the laser positions and DC voltages, we were still unable to trap. We then decided to check whether our oven was producing

strontium. To check whether our oven was producing strontium neutrals, we first shone the 460nm laser through the trapping area, and then turned the oven on to 6A. If the oven is producing strontium, after 10 seconds or so the strip of the image where the 460nm laser is will increase in brightness. We discovered that our oven was indeed producing strontium, so something else must be wrong.

We warmed up the cryostat again and tested the RF with a scope probe near the trap. The RF was also working, so we decided to replace the fiber-integrated trap with a trap we knew worked to test the cryostat system as a whole. We have not yet been able to trap ions with a trap we know works, because we keep shorting the traps and destroying them, but otherwise the cryostat system seems to be working. This means that we can not determine whether the problems we had trapping ions were inherent to the fiber-integrated trap.

5.3   Measurement and Errors

To measure the amount of light from the ion picked up by the fiber, we mounted a PMT and 422nm filter in a light-tight box with an input port for the fiber. The photons from the fiber are measured by the PMT, which detects photons hitting a photocathode by the electrons which are produced by the photoelectric effect. These electrons are then multiplied by a series of dynodes, and are then sent to an FPGA which counts the photons and outputs the counts to software.

Even though we were unable to trap ions, we were still able to perform a test of the light collection abilities of the fiber. There was a large scatter spot on the trap near where we would normally trap ions, which is very bad for ion trapping, but allowed us to test our fiber's light collection. Scatter spots are usually either pieces of dust or places where the gold surface is very non-uniform. When the 422nm laser hits one of these spots, it scatters light in random directions. Figure 5-9 shows a picture taken with the camera of the trap surface with a few scatter spots.

We measured the rate of photons detected with the laser beam hitting the scatter spot as well as with the laser beam blocked. Unfortunately, because scatter spots

Figure 5-9: Trap surface with scatter spots.
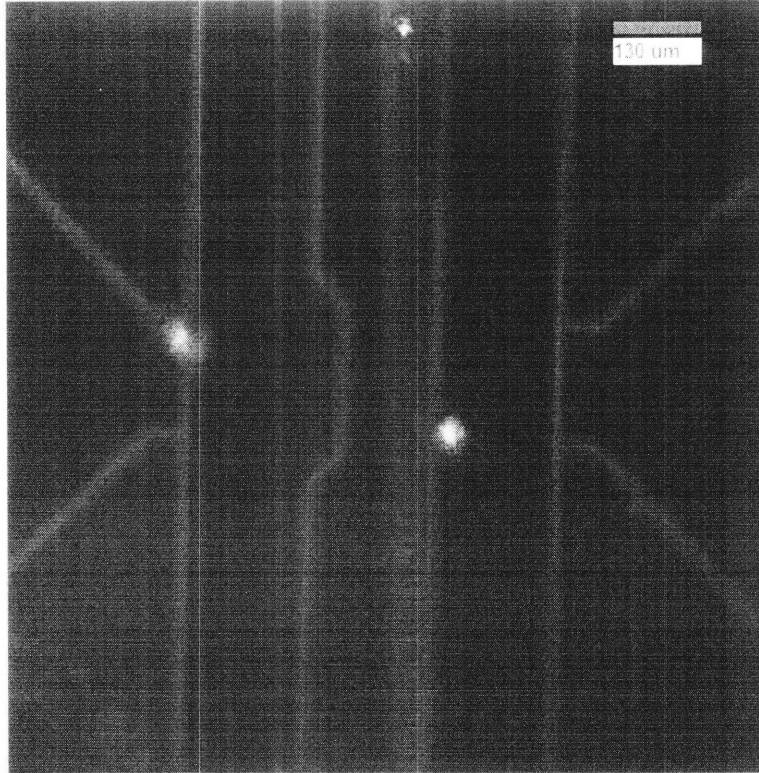
are not isotropic emitters, and the scatter spot was not aligned with the fiber, the efficiency of the of the fiber light collection optics could not be compared with the traditional optics we used. Chapter 6 presents the results of this measurement.

Photon scattering is a Poisson process, so we expect the error on each measurement to be $\sqrt{N}$ where N is the number of counts.

Chapter 6

Results

Although we were unable to trap any ions, we were still able to learn some useful things about optical fiber integration from this experiment. Section 6.1 discusses the results of fiber integration, and section 6.2 discusses the light collection abilities of our fiber on the planar ion trap.

6.1   Fiber Integration

The integration of optical fibers on planar ion traps was somewhat successful. We developed a fabrication procedure and created fiber alignment structures that were both very easy to use and fairly robust. However, one structures did fail under extreme temperature cycling between 77K and 333K (60°C), and separated from the trap. Our scheme for getting fibers into the cryostat worked extremely well. After cooling the cryostat we achieved a pressure of $5.0 \cdot 10^{-8}$ torr, which is well below the pressure that we usually trap ions at. This indicates that the fiber feed-through we designed and built works well enough for regular use in this cryostat.

We were not able to trap ions. This indicated that either the ion trap was not functioning properly, or the amount of dielectrics on the surface of the trap was large enough that charging caused a distortion of the trapping potential to the point that there was no longer a potential well for the ions to be trapped in. See sections 2.1.1 and 2.1.2.

6.2   Fiber Light Collection

We tested our fiber light collection by measuring the counts on the PMT both with the 422nm laser hitting a scatter spot on the surface of the trap, as described in section 5.3. Figure 6-1 is a plot of photons/s received by the PMT vs. time. The average photons received while the laser was on and hitting the scatter spot was $(4.8 \pm .1) \cdot 10^5$ photons/s. The average photons received while the laser was not hitting the scatter spot was 230 ± 40 photons/s. At the beginning of the data collection, there is a small spike above the light from the scatter spot of 5 ± 3 photons/s. We are unsure of what this is, but we think a small particle inside the cryostat flew through the laser beam in the fiber collection area, and scattered an additional amount of light.
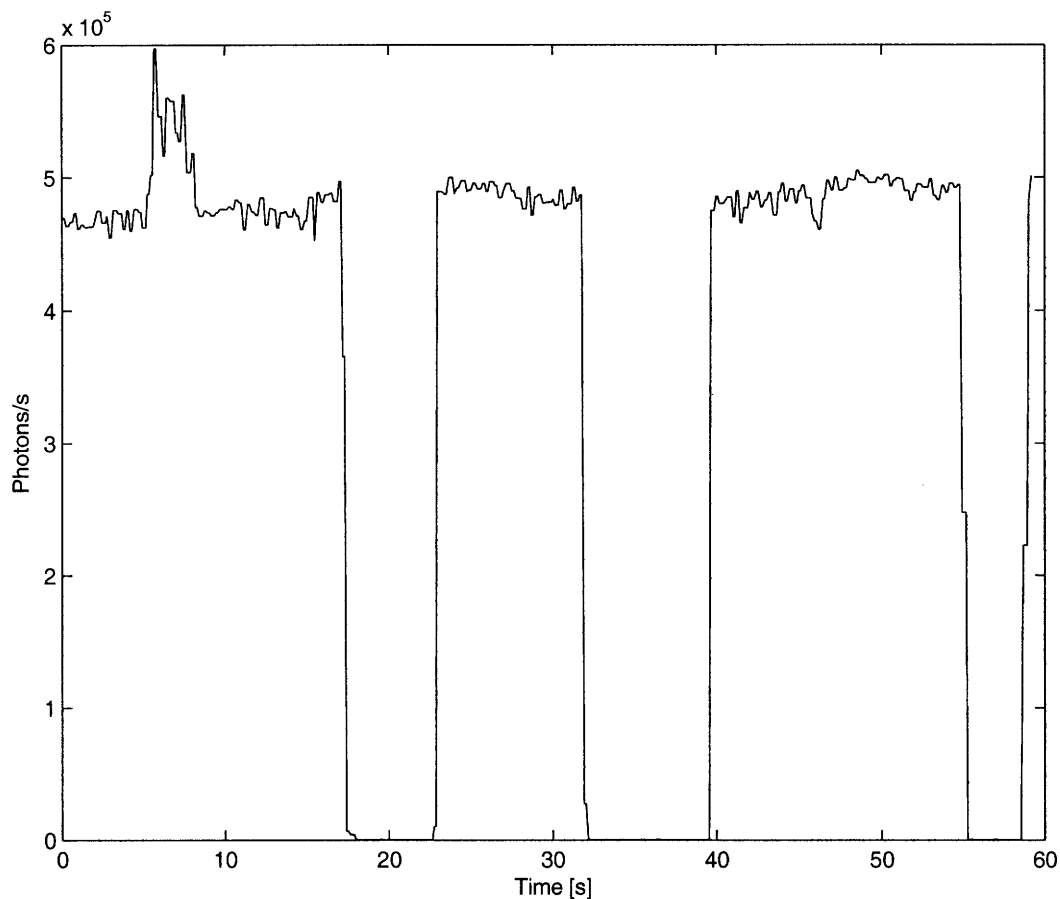

Figure 6-1: Rate of photons received as a function of time with 422nm laser on (and hitting a scatter spot) and off. The small spike at the beginning may be a particle flying through the field of view of the fiber.

With the fiber at a distance of 650 μm from the ion, if we had a trapped ion we

would expect the fiber to collect about $1.2 \cdot 10^5$ photons/s. After taking into account the losses in the fiber connections (78% efficiency) and the PMT efficiency (21%) we expect to detect about $2 \cdot 10^4$ photons/s. With such a large scatter spot on the trap, a trapped ion would barely be above the statistical noise in the photon scattering rate.

The data we collected shows two things. The first is that our fiber on an ion trap can collect light scattered in its field of view. The second is that even though the dark count of the setup is very low (230 ± 40 photons/s) which allows us to do measurements very quickly, the optical fiber is very sensitive to scatter spots. The high background that is associated with scatter spots would statistically force us to measure for a very long time to be able to distinguish whether or not we had an ion if there were also a scatter spot in the field of view of the fiber. In contrast, with our traditional optics we can pinhole down the light from the imaging optics to view only a 50μm x 50μm area, which means that light from scatter spots far from the ion is not detected. Because ion traps never have perfectly smooth and scatter-free surfaces, being able to still do measurements despite the presence of scatter spots on the trap surface is very important. Section 7.2.1 discusses one way to get around the problem of scatter spots on the trap surface interfering with measurements.

Chapter 7

Conclusion

7.1 In this Work

In this thesis, we have explored the design and implementation of optical fiber integration on planar ion traps for light collection. We successfully integrated fiber optics into our cryostat using a fiber feed-through we designed and constructed, modified heat filters, and a fiber connector mating sleeve.

We developed a fabrication procedure of creating fiber alignment structures on ion traps using SU-8 2100 photo-resist, and successfully integrated a fiber onto the trap surface. We were unable to trap ions in our trap, which indicates that either something was wrong with the trap, or the large amount of dielectrics on the surface of the trap due to the fiber and alignment structure charged up and distorted the trapping potential. This indicates that the design may need to be modified to minimize dielectrics on the surface of the trap.

We were able to collect light scattered from the trap with our integrated fiber, which shows promise for fiber based ion detection. However, we discovered that the optical fiber integration scheme we developed is extremely sensitive to scatter spots, which indicated that a design revision may be in order for this fiber based ion detection to be useful for regular use in ion trapping experiments. Section 7.2.1 describes a possible design revision.

Fiber optic integration on planar ion traps is necessary to make ion trap systems

a scalable platform for quantum computation. This thesis began to explore possible ways of integrating fibers on planar ion traps, and showed promise for fiber based ion detection.

7.2 Future Work

Some of the issues we encountered with fiber optic integration on planar ion traps were large amounts of dielectric on the surface of or the trap possibly distorting the trapping potential, and high sensitivity to scatter spots on the surface of the the trap. These problems need to be solved in order for fiber based ion detection to be useful for ion trapping. Section 7.2.1 describes a way to solve these problems as well as conveniently detect ions in multiple trapping sites simultaneously. Section 7.2.2 describes a way to increase the collection efficiency of on-trap fiber optics by increasing the NA of fibers.

7.2.1 Multi-site Through-trap Fiber Optics

One way to solve the problems of large quantities of dielectrics near the trapping site and high sensitivity to scatter spots is to drill holes in the wafer and have the fibers come through the bottom of the trap. This eliminates excess dielectrics on the surface, and ensures that no light will enter the fibers from scatter spots, because the fibers will be pointing upwards.

Consider the trap design in figure 7-1 The small circles in the ground plane are meshed gold, with 50% of the area open to allow photons to pass through. Ions are trapped directly above these circles, and a high NA large core optical fiber is directly below the trap surface. This accomplishes three things. The first is that each fiber can only detect light from one of the trapping sites. (See figure 7-2) The second is that there is a much smaller amount of exposed dielectric on the surface of the trap. The third is that because there is a much smaller amount of dielectric, we can trap ions much closer to the tip of the fiber, which allows for a much higher light collection efficiency.
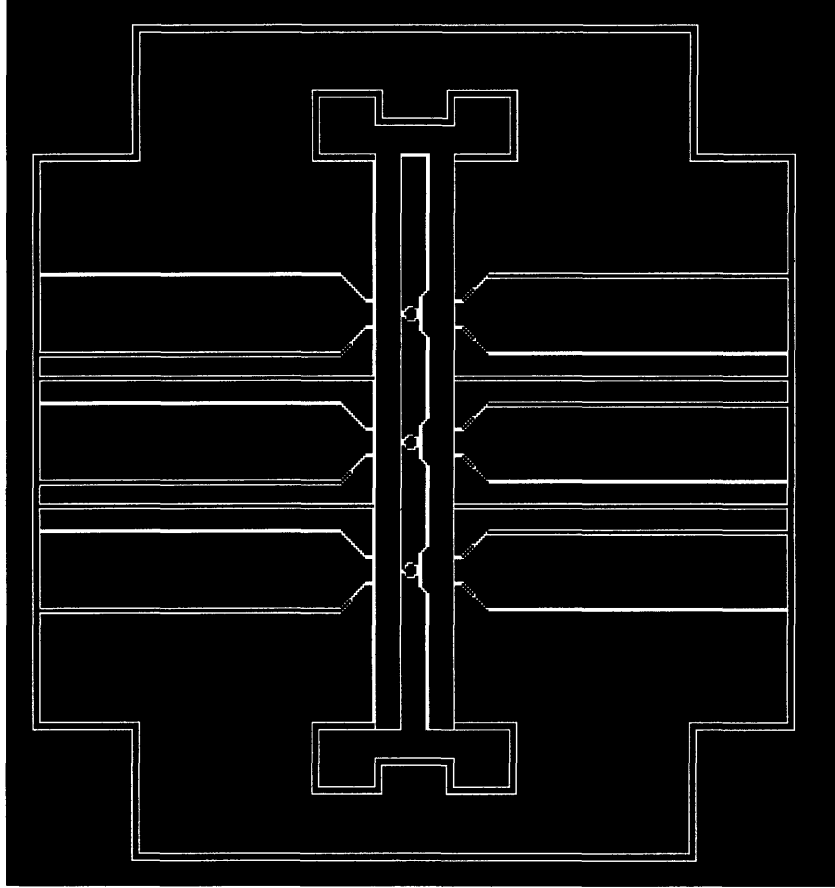
Figure 7-1: Design for a multi-site ion trap. The small circles in the ground plane are meshed gold, with 50% of the area open to allow photons to pass through. Ions are trapped directly above these circles, and a high NA large core optical fiber is directly below the trap surface. This trap can be linearly scaled to almost any size provided the ground plane is at least 75 μm wide.

One way to fabricate this trap would be to start with a 1cm x 1cm square wafer of silicon, grow 5μm of SiO_2 on both surfaces, and then apply photo-resist to the front and back of the fiber. Then, flip the wafer over to be bottom up, expose a mask pattern on the back of the wafer for the fiber holes, develop the resist, and then etch through the back of the wafer using DRIE (deep reactive ion etch). This results in extremely vertical feature walls, which is needed for securing and aligning the fiber. Next,strip all the remaining photo-resist, flip the wafer over again, secure to a dummy wafer using photo-resist, and fabricate the trap structures on the SiO_2 surface. This will result in a trap with "windows" of SiO_2 with gold mesh over them that photons can travel through. Finally, insert the fibers into the trap. Figure 7-3 outlines the
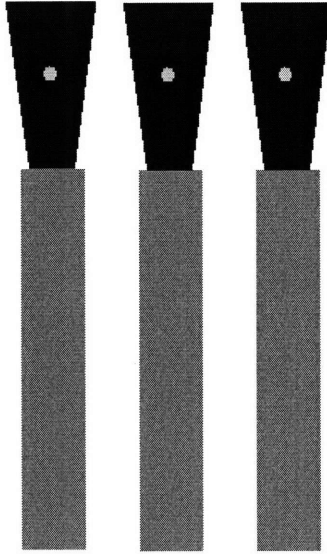
Figure 7-2: Depiction of multiple fibers and their light acceptance cones detecting ions in adjacent trap sites. This diagram is not to scale.

fabrication procedure for creating a multi-site trap with through-trap optical fibers.

7.2.2 Lensed Fibers

High NA fibers combined with the trap design above would greatly improve light collection efficiency. In a trap with an ion height of 100μm, a fiber with a core diameter of 100 μm would require a NA of at least .45 to collect all of the light which intersects the core of the fiber after being scattered from the ion. Larger diameter fibers would require even higher numerical apertures. One way to increase the NA of fibers is to make the indexes of refraction of the core and cladding more dissimilar. Another way to increase the NA of fibers is to lens the ends of the fibers by either melting the ends to introduce a radius of curvature [KK07] or by placing ball lenses in front of the fibers.

Lensed fibers and through-trap fiber optics provide a promising avenue for integration of optical fibers on planar ion traps for fiber-based ion detection. It is worth exploring this option for application to scalable quantum computation.
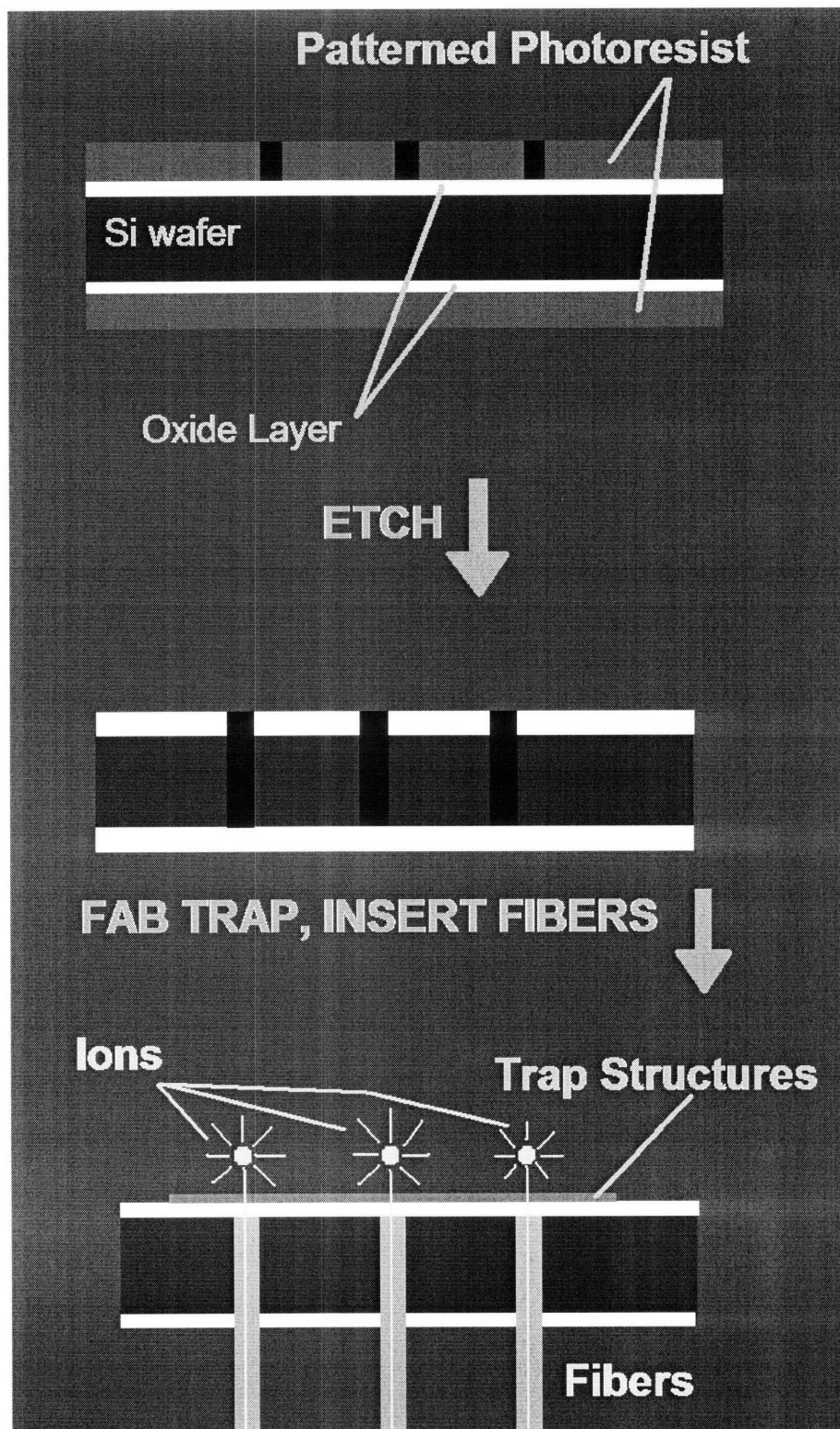
Figure 7-3: Schematic of the fabrication process for creating multi-site through-trap fiber optics. This diagram is not to scale.

Appendix A

Fabrication Procedures

This appendix gives full fabrication procedures for making a planar ion trap with fiber alignment structures.

A.1 Planar Ion Trap

- Wafer preparation: Silver(0.05um)/Ti(75A)/Single crystal quartz (silver is the top layer)

- Bake at 120C for 5 minutes on a hot-plate

- Coat wafer with AZ 4620, spin at 2500 rpm for 10 seconds and 4500 rpm for 60 seconds.

- Bake at 90C in oven for 35 minutes.

- Align mask on wafer.

- Expose at 365nm for 7.5 seconds three times, with a time interval of 30 sec.

- Develop in AZ 440 MIF for 5 minutes.

- Electro-plate at 70C, stirring speed = 300 rpm, current = 10 mA for 20 minutes.

- Rinse with acetone and isopropyl alcohol

- Gold etch for 15 seconds with $NH_4OH:H_2O_2:H_2O = 1:1:4$

- Titanium etch for 15 seconds $HF:H_2O = 1:2$

- Rinse with isopropyl alcohol

A.2 Fiber Alignment Structures

- Attach trap to 3" wafer using a drop of NR7.

- Bake on hot-plate at 95C for 4 minutes.

- Put a few ml of SU-8 2100 on center of trap.

- Center trap on spinner, spin at 1000 rpm for 10 seconds, spin at 2500 rpm for 30 seconds, spin at 700 rpm for 10 seconds.

- Bake on hot-plate at 65C for 7 minutes.

- Bake on hot-plate at 95C for 45 minutes.

- Tape wafer to KS aligner chuck using double-sided tape.

- Adjust height of chuck very carefully. We just barely want contact light to come on when the lever is fully back.

- Align mask to trap.

- Expose at 365nm for 4 minutes.

- Bake on hot-plate at 65C for 6 minutes.

- Bake on hot-plate at 95C for 17 minutes.

- Develop in PM acetate for 4-6 minutes or until unexposed SU-8 is gone.

- Rinse in isopropyl alcohol.

- Dip in acetone for 15 seconds to remove trap from wafer, or use tweezers to pull trap off of the wafer.

- Rinse in isopropyl alcohol.

- Post-bake on hot-plate at 95C for 3 minutes.

Notes: Let trap sit in air for at least 24 hours before attempting to insert the fiber to let the SU-8 fully cure. This procedure should give you an alignment structure height of about 170um.

Bibliography

[BCS+04]   M.D. Barrett, J. Chiaverini, T. Schaetz, J. Britton, W.M. Itano, J.D. Jost, E. Knill, C. Langerand, D. Leibfried, R. Ozeri, and D.J. Wineland. Deterministic quantum teleportation of atomic qubits. *Nature*, 429:737–739, June 2004.

[BKRB08a] J. Benhelm, G. Kirchmair, C.F. Roos, and R. Blatt. Experimental quantum information processing with $^{43}Ca^+$ ions. *arXiv:0804.1261v1*, April 2008.

[BKRB08b] J. Benhelm, G. Kirchmair, C.F. Roos, and R. Blatt. Towards fault tolerent quantum computing with trapped ions. *arXiv:0803.2798v1*, March 2008.

[CBB+05]   J. Chiaverini, R.B. Blakestad, J. Britton, J.D. Jost, C. Langer, D. Leibfried, R. Ozeri, and D.J. Wineland. Surface-electrode architecture for ion-trap quantum information processing. *Quantum Information and Computation*, 5:419–439, 2005.

[CLS+04]   J. Chiaverini, D. Leibfried, T. Schaetz, M.D. Barrett, R.B. Blakestad, J. Britton, W.M. Itano, J.D. Jost, E. Knill, C. Langer, R. Ozeri, and D.J. Wineland. Realization of quantum error correction. *Nature*, 432:602–605, December 2004.

[DBIW89]   F. Diedrich, J.C. Berquist, Wayne M. Itano, and D.J. Wineland. Laser cooling to the zero-point energy of motion. *Physical Review Letters*, 62(4):403–406, January 1989.

[Gho95]   Pradip K. Ghosh. *Ion traps*. Oxford University Press, New York, 1995.

[GT98]   A. Ghatak and K. Thyagarajan. *An Introduction to Fiber Optics*. Cambridge University Press, 1998.

[HRW07]   D.B. Hume, T. Rosenband, and D.J. Wineland. High-fidelity adaptive qubit measurements through repetitive information transfer. *Physical Review Letters*, 99, 2007.

[IJW87]   Wayne M. Itano, J.C.Bergquist, and D.J. Wineland. Laser spectroscopy of trapped atomic ions. *Science*, 237(4815):612, August 1987.

[KK07]   Jungsang Kim and Changsoon Kim. Integrated optical approach to trapped ion quantum computation. *arXiv:0711.3866v1*, November 2007.

[L+05]   Xiyuan Liu et al. Fabrication of alignment structures for a fiber resonator by use of deep-ultraviolet lithography. *Applied Optics*, 44(32):6857–6860, November 2005.

[Lab08]   Jaroslaw Labaziewicz. *Scalable Ion Traps for Trapped Ion Quantum Computation*. PhD dissertation, Massachusetts Institute of Technology, Department of Physics, July 2008.

[LGA+08]   Jaroslaw Labaziewicz, Yufei Ge, Paul Antohi, David Leibrandt, Kenneth R. Brown, and Isaac L. Chuang. Suppression of heating rates in cryogenic surface-electrode ion traps. *Physical Review Letters*, 100:013001, January 2008.

[PLB+06]   C. E. Pearson, D. R. Leibrandt, W. S. Bakr, W. J. Mallard, K. R. Brown, and I. L. Chuang. Experimental investigation of planar ion traps. *Physical Review A*, 73:32307, 2006.

[POF58]   W. Paul, O. Osberghaus, and E. Fisher. Fort. des wirt. und verkher. *Nordrhein-Westfalen*, (415), 1958.

[Ric05]   Philip Richerme. Depletion, quantum jumps, and temperature measurements of ^{88}Sr$^+$ ions in a linear paul trap. Bachelor's thesis, Massachusetts Institute of Technology, Physics Department, June 2005.

[RSI+07]   T. Rosenband, P.O. Schmidt, W.M. Itano, T.M. Fortier, J.E. Stalnaker, K. Kim, S.A. Diddams, J.C.J. Koelemij, J.C. Bergquist, and D.J. Wineland. Observation of the ^{1}S$_0$–^{3}P$_0$ clock transition in ^{27}Al$^+$. *Physical Review Letters*, 98, 2007.

[S+06]   S. Seidelin et al. A microfabricated surface-electrode ion trap for scalable quantum information processing. *Physical Review Letters*, 96, 2006.

[She08]   Ruth Shewmon. 5S$_{1/2}$ − 4D$_{5/2}$ transition of ^{88}Sr$^+$ as an optical qubit. Bachelor's thesis, Massachusetts Institute of Technology, Physics Department, June 2008.

[W+03]   D.J. Wineland et al. Quantum information processing with trapped ions. *Phil. Trans. Royal Soc. London A*, 361, 2003.

[WMI+98]   D.J. Wineland, C. Monroe, W.M. Itano, D. Leibfried, B.E. King, and D.M. Meekof. Experimental issues in coherent quantum manipulation of trapped atomic ions. *Journal of Research of the National Institute of Standards and Technology*, 103(3):259–328, May 1998.